

Syngas-to-C₂ oxygenates on Cu-based catalyst: Quantitative insight into the balancing effect of active Cu^{δ+} (0 ≤ δ ≤ 1) sites

Cong Wei^a, Riguang Zhang^{a,*}, Lixia Ling^a, Debao Li^b, Bo Hou^b, Baojun Wang^{a,*}

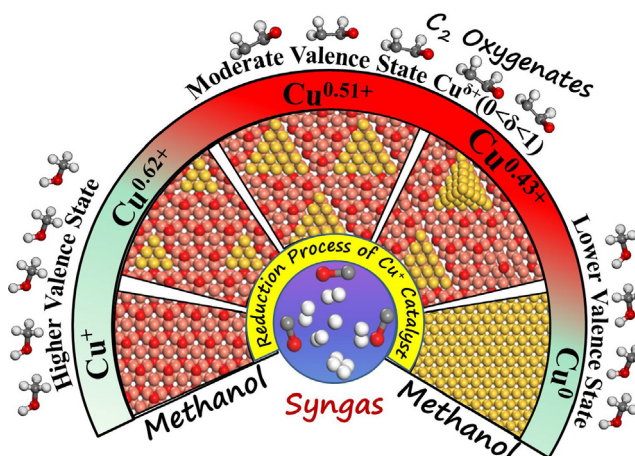
^a Key Laboratory of Coal Science and Technology of Ministry of Education and Shanxi Province, Taiyuan University of Technology, Taiyuan 030024, Shanxi, PR China

^b State Key Laboratory of Coal Conversion, Institute of Coal Chemistry, Chinese Academy of Sciences, Taiyuan 030001, Shanxi, PR China

HIGHLIGHTS

- The precise role of Cu^{δ+} (0 ≤ δ ≤ 1) sites is quantitatively revealed in syngas-to-C₂ oxygenates.
- The Cu⁺ and Cu⁰ sites dominantly contribute to the conversion of syngas to form methanol.
- The moderate valence state (0.43 and 0.51) Cu^{δ+} (0 < δ < 1) sites mainly catalyze syngas-to-C₂ oxygenates.
- The redox properties of Cu₂O should be enhanced to form moderate valence state Cu^{δ+} (0 < δ < 1) sites.
- The electronic properties well illustrate the precise role of Cu^{δ+} (0 ≤ δ ≤ 1) sites.

GRAPHICAL ABSTRACT



ARTICLE INFO

Article history:

Received 21 March 2020
 Received in revised form 5 May 2020
 Accepted 7 May 2020
 Available online 16 May 2020

Keywords:

Syngas conversion
 C₂ oxygenates
 Cu catalyst
 Active sites
 Valence state
 Density functional theory

ABSTRACT

Cu-based catalysts can experimentally catalyze the conversion of syngas-to-C₂ oxygenates, however, since the chemical state of Cu sites dynamically evolves in the reaction process, no consensus has been reached on the precise roles of active Cu^{δ+} (0 ≤ δ ≤ 1) sites. Here we resolve this long-term dispute with a series of highly comparable Cu catalyst. The results for the first time quantitatively identify the precise role of Cu^{δ+} (0 ≤ δ ≤ 1) sites in adjusting the catalytic activity and selectivity of syngas conversion over Cu-based catalysts, which is well illustrated in the view of electronic properties. Our quantitative results show that the moderate valence state Cu^{δ+} (δ = 0.43 and 0.51) sites can highly-active and highly-selective catalyze the conversion of syngas to produce C₂ oxygenates, which is also indirectly supported by the reported experiment studies. It is proposed that the balancing effect of Cu⁰ and Cu⁺ species in the experiment contribute to high catalytic performance toward the formation of C₂ oxygenates.

© 2020 Elsevier Ltd. All rights reserved.

1. Introduction

C₂ oxygenates (typically such as ethanol) formed by syngas (CO + H₂) is thought to be a promising approach, which can convert carbon dioxide, natural gas, biomass and coal into high value-added chemicals (Hindermann et al., 1993; Subramani and

* Corresponding authors.

E-mail addresses: zhangriguang@tyut.edu.cn (R. Zhang), wangbaojun@tyut.edu.cn, wbj@tyut.edu.cn (B. Wang).

Gangwal, 2008; Chuang et al., 1985; Pan et al., 2007). Nowadays, Rh-based catalysts have presented effectively catalytic performance toward the conversion of syngas to produce C₂ oxygenates, however, the poor CO conversion rate and few storage quantities of noble metal Rh hinder its wide utilization in industry (Pan et al., 2007; Mei et al., 2010; Subramanian et al., 2010; Mo et al., 2009; Haider et al., 2009). Alternatively, a low cost Cu-based catalysts, the easier modification with transition metals and the high CO conversion rate, are commonly used in the conversion of syngas to produce C₂ oxygenates (Sun et al., 2016; Yue et al., 2014; Gupta et al., 2011; Su et al., 2016; Prieto et al., 2014; Zhang et al., 2019). However, the Cu-based catalysts previously employed in syngas conversion to ethanol lead to a rapid decrease of ethanol selectivity due to the change of active phase in the reduction and reaction processes (Gupta et al., 2011; Su et al., 2016; Prieto et al., 2014; Wang et al., 2017; Xiang et al., 2015; Morrill et al., 2013); which limited its further industrial applications. Thus, the deeper understandings that how do the Cu-based catalysts work under the realistic conditions become very necessary for the rational design of Cu-based catalyst. In addition, two critical steps for the conversion of syngas to C₂ oxygenates on the Rh-based and Cu-based catalysts have been generally accepted (Hindermann et al., 1993; Zhang et al., 2019; Zhao et al., 2011; Schumann et al., 2018; Choi and Liu, 2009); the first is to produce the key CH_x (x = 1–3) intermediates, the second is the carbon chain formation of C₂ oxygenates.

The present understanding about the active phase of Cu-based catalyst in the conversion of syngas to produce C₂ oxygenates mainly concentrated on the Cu⁺, Cu^{δ+} (0 < δ < 1) and Cu⁰ species due to the easier reduction of Cu²⁺ species under the reducing atmosphere and at the temperature of 500–623 K (Maimaiti et al., 2014; Zuo et al., 2013; Li et al., 2019), for example, the systematical investigations by Maimaiti et al. (2014) revealed that the CuO can be reduced to Cu₂O at approximately 360 K and ultimately be reduced to metal Cu at 780 K. Meanwhile, several excellent studies showed that the Cu⁺, Cu^{δ+} (0 < δ < 1) and Cu⁰ species always co-exist on the Cu-based catalysts, especially, the chemical state of Cu species in the Cu-based catalysts dynamically evolves during the process of the reaction (Kuld et al., 2016; Eren et al., 2015; Yue et al., 2013), such as, Li et al. (2019) found that the peaks of Cu₂O were significantly weakened, accompanied by the Cu diffraction peaks obviously sharpened as the ethanol production from syngas over the Cu-based catalysts, indicating that Cu particles aggregate during the reaction process. Further, the experiment and theoretical studies by Tissot et al. (2019) clearly presented the reduction process of Cu₂O surfaces under the hydrogen-rich reducing atmosphere, firstly, a large number of OH species were observed on the Cu₂O surface, subsequently, a large number of metal Cu clusters appeared on the catalyst surface, which were attributed to that H takes away the O on the Cu₂O surface, resulting in the oxygen vacancies formation and the reconstruction of surface Cu atoms to Cu clusters. Moreover, the phenomenon that the specifically designed Cu/Cu₂O interface is more active for the reduction of CO₂ to methanol was reported by Chang et al. (2018). It is concluded that Cu₂O catalyst under the reducing atmosphere firstly go through the formation of surface oxygen vacancies, which promotes the reorganization of the surface Cu atoms; subsequently, the surface Cu atoms are aggregated to form the Cu/Cu₂O interfaces or completely reduced to form metal Cu cluster along with the progress of the reaction.

As mentioned above, since different active phases of Cu catalyst co-exist and evolve dynamically during the reaction process, it is very difficult to quantitatively identify the precise roles of Cu⁺, Cu^{δ+} (0 < δ < 1) and Cu⁰ species, and the attribution of active phase for the Cu catalyst remains controversial yet (Kuld et al., 2016; Sá et al., 2010; Gokhale et al., 2008; Behrens, 2012; Cant

et al., 1985; Chung et al., 1992), for example, the Cu⁰ species is considered to be the active phase in the hydrogenation reactions of DMO (Zhao et al., 2013; Yin et al., 2009; Yin et al., 2010; Yin et al., 2008; Gong et al., 2012) or DME (San et al., 2009), whereas the Cu⁺ species is acted as the active phase for ethanol formation from CO (Zuo et al., 2013; Li et al., 2019; Sun et al., 2019) or DMO (He et al., 2011) hydrogenation; meanwhile, the considerable researches about the hydrogenation reactions showed that there may be a synergetic effect of the Cu⁰ and Cu⁺ species, i.e. Cu^{δ+} (0 < δ < 1) species (Yue et al., 2013; Wang et al., 2015; Zheng et al., 2015), such as, Wang et al. (2015) found that the appropriate ratio of Cu⁺ and Cu⁰ species enhanced the activity of DMO hydrogenation to form ethanol over the Cu/SiO₂ catalysts. The similar results were drawn by Zheng et al. (2015) that the imbalance distribution of the Cu⁺ and Cu⁰ species leads to the rapid decrease of ethanol selectivity in DMO hydrogenation. Further, the interface between the Cu⁺ species and the highly dispersed CuO_x (x = 0.2–0.5) species was observed to be more active for CO oxidation (Eren et al., 2015; Wang et al., 2015). Therefore; above analysis show that different valence states of Cu catalysts as the active sites exhibit important role in the hydrogenation reactions related to the C–O bond, as a result, for the conversion of syngas to produce C₂ oxygenates, the deep insights into the catalytic performance of Cu catalysts with different valence states would be significant for revealing the precise roles of Cu⁺, Cu^{δ+} (0 < δ < 1) and Cu⁰ as the active sites.

Further, the experiment by Li et al. (2019) revealed that the Cu⁺ site is beneficial to the formation of CH₃OH in syngas conversion; the Cu^{δ+} (0 < δ < 1) sites between Cu⁰ and Cu⁺ species effectively increase ethanol selectivity. Theoretically, numerous studies about the conversion mechanism of syngas-to-C₂ oxygenates have been carried out on the (1 1 1) (Sun et al., 2013; Sun, 2013); (2 1 1) (Zhang et al., 2013); (1 1 0) (Sun, 2013; Zhang et al., 2013) and (1 0 0) (Sun, 2013; Zheng et al., 2015) surfaces of Cu⁰ species as the active sites, methanol is the dominant product. Thus, the Cu^{δ+} (0 < δ < 1) sites with both Cu⁰ and Cu⁺ species simultaneously as the active sites should play a crucial role to modulate the catalytic performance of Cu catalyst toward C₂ oxygenates synthesis from syngas. Especially, for the Cu^{δ+} (0 < δ < 1) sites with the metastable state structure, the studies by Greiner et al. (2017) believed that the catalyst materials in the presence of the metastable state are close to a thermodynamic phase transition, which presents distinct catalytic performance. However, up to now, the quantitative insight into the precise role of Cu^{δ+} (0 < δ < 1) sites in catalyzing the conversion of syngas-to-C₂ oxygenates are still lacking in the theoretical and experimental studies, and what is the precise valence state of Cu^{δ+} (0 < δ < 1) sites to exhibit excellent catalytic performance toward the syngas-to-C₂ oxygenates.

In this study, focusing on quantitatively identifying the precise role of Cu species with different valence states as the active sites in the conversion of syngas-to-C₂ oxygenates, here, the metal Cu and Cu₂O are used to simulate the Cu catalyst corresponding to the Cu⁰ and Cu⁺ species acted as the active sites, respectively; meanwhile, three mixed Cu₂O_x model surfaces are constructed to simulate the Cu catalyst with different metastable state Cu^{δ+} (0 < δ < 1) structure as the active site based on a reducible support. Then, DFT calculations with microkinetic modeling are employed to fully investigate the mechanism of syngas conversion to produce C₂ oxygenates on the Cu⁺ and Cu^{δ+} (0 < δ < 1) species as the active site, and compared with the previous work of Cu⁰ species, which can reflect the effect of Cu valence state on the catalytic performance under the reducing conditions. Finally, the differential charge density, Bader charge and density of states are fully analyzed to obtain the relationship between the electronic properties of Cu^{δ+} (0 ≤ δ ≤ 1) sites and the catalytic performance for the conversion reaction of syngas to produce C₂ oxygenates.

2. Computational methods

2.1. Surface model

Cu_2O catalyst is selected to model Cu^+ active sites, the (1 1 1) surface was extensively considered as an ideal model of Cu_2O catalysts due to its higher stability, larger surface ratio and the most catalytically active obtained in the theoretical (Islam et al., 2009; Sun et al., 2008; Sun et al., 2007) and experimental studies (Schulz and Cox, 1991; Lin et al., 1992; Ønsten et al., 2009; Bendavid and Carter, 2013; Niluis et al., 2016; Bendavid and Carter, 2013; Huang, 2016), moreover, the presence of coordination unsaturated Cu^+ active sites can enhance the adsorption ability of key intermediates (Huang, 2016; Yang et al., 2018). Our results also showed that the coordination-unsaturated Cu^+ site has strong adsorption ability for the key intermediates (CO, CHO, CH_2O , CH_3O , CHO and CH_2OH) in CO activation to form CH_x species (see Table S1). Thus, the $\text{Cu}_2\text{O}(1\ 1\ 1)$ surface (named as $\text{Cu}_2\text{O}(1\ 1\ 1)$) is used to simulate the Cu^+ active sites (see Fig. 1a).

Since the surfaces structure of metal oxides usually present the surface vacancies under the realistic conditions, and therefore affect its catalytic performance, such as surface reactivity (Yin et al., 2007). For the $\text{Cu}_2\text{O}(1\ 1\ 1)$ surface, it can be partially reduced to yield the surface oxygen-vacancy in the reducing atmosphere, resulting in the formation of the metastable $\text{Cu}^{\delta+}(0 < \delta < 1)$ struc-

ture; meanwhile, previous studies showed that the loss of all $\text{Cu}_2\text{O}(1\ 1\ 1)$ surface oxygen atoms is thermodynamically favored (Nie et al., 2014). Zhang et al. (2013, 2011, 2010) proved that the $\text{Cu}_2\text{O}(1\ 1\ 1)$ with oxygen-vacancy presents better catalytic activity for the adsorption and dissociation of O_2 , H_2 , H_2O and H_2S species. Thus, the $\text{Cu}_2\text{O}(1\ 1\ 1)$ with oxygen-vacancy is applied to investigate the effect of the metastable $\text{Cu}^{\delta+}(0 < \delta < 1)$ sites on the formation of CH_x and C_2 oxygenates in this study, as shown in Fig. 1b and 1c, the $\text{Cu}_2\text{O}(1\ 1\ 1)$ with oxygen-vacancy are established by removing one and two surface O_{suf} atoms corresponding to the content of 25% and 50% surface oxygen-vacancy, named as $\text{Cu}_2\text{O}(1\ 1\ 1)-\text{O}_{\text{v}25}$ and $\text{Cu}_2\text{O}(1\ 1\ 1)-\text{O}_{\text{v}50}$ surfaces, respectively, in which the coordination-unsaturated Cu is assumed to be the $\text{Cu}^{\delta+}(0 < \delta < 1)$ site. Obviously, the oxygen vacancies induce the reconstruction of surface Cu atoms to form the surface Cu clusters (Chang et al., 2018; Yang et al., 2018).

As mentioned above, along with the formation of more oxygen-vacancies over the $\text{Cu}_2\text{O}(1\ 1\ 1)$ surface, the reconstruction of surface Cu atoms leads to their aggregation to form the Cu/ Cu_2O interfaces or further be completely reduced to form the metal Cu under the reducing atmosphere. Thus, the reconstruction of surface Cu atoms to form the Cu/ Cu_2O interfaces is considered to be the metastable $\text{Cu}^{\delta+}(0 < \delta < 1)$ active site, as shown in Fig. 1d, a tetrahedron Cu_4 cluster was adsorbed on the $\text{Cu}_2\text{O}(1\ 1\ 1)-\text{O}_{\text{v}50}$ surface (named as Cu/ $\text{Cu}_2\text{O}(1\ 1\ 1)-\text{O}_{\text{v}50}$), where the coordination-unsaturated Cu at

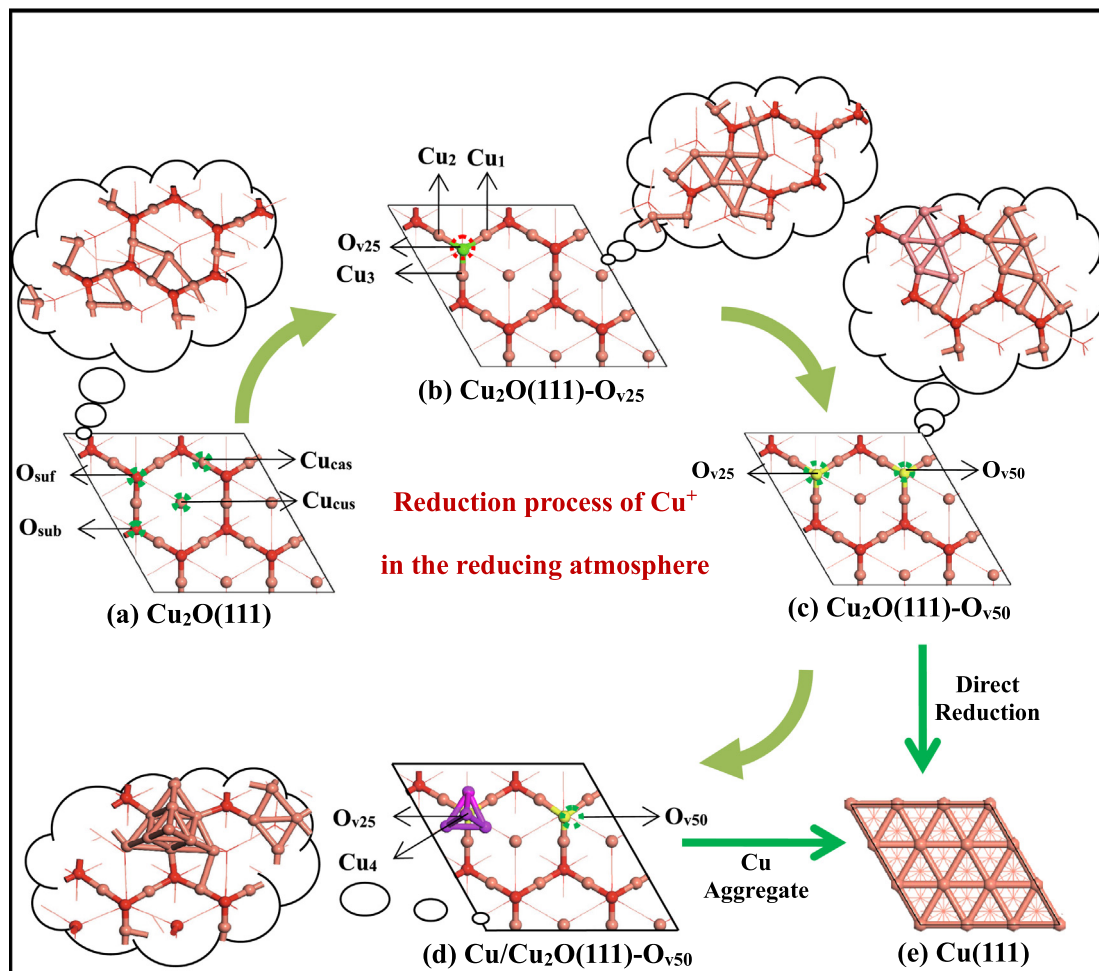


Fig. 1. Surface morphology of $\text{Cu}_2\text{O}(1\ 1\ 1)$ surface (a) perfect, (b) one oxygen-vacancy, (c) two oxygen-vacancy, (d) Cu_4 supported over two oxygen-vacancy, and (e) the Cu (1 1 1) surface, which are named as $\text{Cu}_2\text{O}(1\ 1\ 1)$, $\text{Cu}_2\text{O}(1\ 1\ 1)-\text{O}_{\text{v}25}$, $\text{Cu}_2\text{O}(1\ 1\ 1)-\text{O}_{\text{v}50}$, Cu/ $\text{Cu}_2\text{O}(1\ 1\ 1)-\text{O}_{\text{v}50}$ and Cu(1 1 1) surfaces, respectively. The red, orange and pink balls denote O, Cu atoms and the Cu atoms of Cu_4 cluster, respectively. (For interpretation of the references to colour in this figure legend, the reader is referred to the web version of this article.)

the interface is assumed to be the $\text{Cu}^{\delta+}$ ($0 < \delta < 1$) active site. In addition, the Cu_4 cluster in both three-dimensional and two-dimensional configurations are considered to model the aggregation of Cu^0 , the three-dimensional Cu_4 cluster not only has higher stability than the two-dimensional one, but also represent the smallest unit of a three-dimensional configuration that can reflect both interactions of metal–metal and metal-support (Zhang et al., 2012; Zhang et al., 2011). The $\text{Cu}(1\ 1\ 1)$ surface is selected to simulate the Cu^0 active sites (Sun et al., 2013; Sun, 2013), as shown in Fig. 1e.

Further, in order to verify the existence of the metastable $\text{Cu}^{\delta+}$ ($0 < \delta < 1$) structures on the $\text{Cu}_2\text{O}(1\ 1\ 1)\text{-O}_{v25}$, $\text{Cu}_2\text{O}(1\ 1\ 1)\text{-O}_{v50}$ and $\text{Cu}/\text{Cu}_2\text{O}(1\ 1\ 1)\text{-O}_{v50}$ surfaces (Fig. 1b–d), the analysis of the electronic properties is carried out, as presented in Fig. 2a, the overlap between O_{2p} and Cu_{3d} , the differential charge (details in Fig. S1) between the coordination-unsaturated Cu and its adjacent O atoms for the $\text{Cu}_2\text{O}(1\ 1\ 1)\text{-O}_{v25}$, $\text{Cu}_2\text{O}(1\ 1\ 1)\text{-O}_{v50}$ and $\text{Cu}/\text{Cu}_2\text{O}(1\ 1\ 1)\text{-O}_{v50}$ surfaces are lower than those of the $\text{Cu}_2\text{O}(1\ 1\ 1)$ surface, suggesting that the interaction between Cu and O atoms on the $\text{Cu}_2\text{O}(1\ 1\ 1)\text{-O}_{v25}$, $\text{Cu}_2\text{O}(1\ 1\ 1)\text{-O}_{v50}$ and $\text{Cu}/\text{Cu}_2\text{O}(1\ 1\ 1)\text{-O}_{v50}$ surfaces is weaker than that on the $\text{Cu}_2\text{O}(1\ 1\ 1)$ surface, which is also confirmed by the results of Bader charges of Cu (0.33, 0.27, 0.23 vs. 0.52 e) and the Cu–O bond lengths (1.949, 1.966, 1.974 vs. 1.930 Å) (see Fig. 2b). Correspondingly, the coordination-unsaturated Cu exists in the form of the metastable $\text{Cu}^{\delta+}$ ($0 < \delta < 1$) sites over the $\text{Cu}_2\text{O}(1\ 1\ 1)\text{-O}_{v25}$, $\text{Cu}_2\text{O}(1\ 1\ 1)\text{-O}_{v50}$ and $\text{Cu}/\text{Cu}_2\text{O}(1\ 1\ 1)\text{-O}_{v50}$ surfaces.

Finally, to further quantitatively obtain the precise valence state of the metastable $\text{Cu}^{\delta+}$ ($0 < \delta < 1$) sites corresponding to the $\text{Cu}_2\text{O}(1\ 1\ 1)\text{-O}_{v25}$, $\text{Cu}_2\text{O}(1\ 1\ 1)\text{-O}_{v50}$ and $\text{Cu}/\text{Cu}_2\text{O}(1\ 1\ 1)\text{-O}_{v50}$ surface models, the relationship between the Bader charge and the valence state of $\text{Cu}^{\delta+}$ ($0 \leq \delta \leq 1$) sites over the $\text{Cu}_2\text{O}(1\ 1\ 1)$, $\text{Cu}_2\text{O}(1\ 1\ 1)\text{-O}_{v25}$, $\text{Cu}_2\text{O}(1\ 1\ 1)\text{-O}_{v50}$, $\text{Cu}/\text{Cu}_2\text{O}(1\ 1\ 1)\text{-O}_{v50}$ and $\text{Cu}(1\ 1\ 1)$ surfaces are obtained (see Fig. S2). Our results show that the $\text{Cu}^{\delta+}$ ($0 \leq \delta \leq 1$) sites over the $\text{Cu}_2\text{O}(1\ 1\ 1)$, $\text{Cu}_2\text{O}(1\ 1\ 1)\text{-O}_{v25}$, $\text{Cu}_2\text{O}(1\ 1\ 1)\text{-O}_{v50}$, $\text{Cu}/\text{Cu}_2\text{O}(1\ 1\ 1)\text{-O}_{v50}$ and $\text{Cu}(1\ 1\ 1)$ surfaces correspond to the precise valence states of 0.99, 0.62, 0.51, 0.43 and -0.06 , respectively, in which the valence states of 0.99 and -0.06 for the $\text{Cu}_2\text{O}(1\ 1\ 1)$ and $\text{Cu}(1\ 1\ 1)$ surfaces are nearly close to the valence state of Cu^+ and Cu^0 sites, respectively.

Therefore, in this study, the $\text{Cu}(1\ 1\ 1)$ surface is selected to simulate the Cu^0 active sites. Four types of $\text{Cu}_2\text{O}(1\ 1\ 1)$ surfaces, the

perfect, 25% and 50% surface oxygen-vacancies, as well as Cu_4 cluster adsorbed over the 50% oxygen-vacancies surfaces, have been employed to simulate the Cu^+ and $\text{Cu}^{\delta+}$ ($0 < \delta < 1$) active sites, a $p(2 \times 2)$ supercell slab model with eight atomic layers separated by 15 Å vacuum is employed for these $\text{Cu}_2\text{O}(1\ 1\ 1)$ surfaces, in which the adsorbed species and the upper six atomic layers of the slab model are allowed to relax, while the bottom two atomic layers of the slab model are fixed.

2.2. Calculation methods

All calculations of the adsorption and reaction are implemented by spin-polarized density functional theory (DFT) using Dmol³ code in Material Studio 8.0. The generalized gradient approximation (GGA) with the Perdew–Burke–Ernzerhof (PBE) is implemented for the electronic exchange and correlation (Delley, 1990; Tian et al., 2007). Effective Core Potentials (ECP) is set, and the double numerical plus polarization (DNP) basic set is used developed (Delley, 1990; Tian et al., 2007; Zhou et al., 2007). The energy convergence, maximum force and maximum distance are set at 2.0×10^{-6} Ha, 2.0×10^{-3} Ha·Å⁻¹ and 5.0×10^{-3} Å, respectively. A Monkhorst–Pack with $3 \times 3 \times 1$ k -point mesh sampling is employed in the surface Brillouin zone, a Methfessel–Paxton smearing of 0.005 Ha is employed to accelerate convergence. The transition state (TS) is obtained using the complete LST/QST method (Halgren and Lipscomb, 1977; Govind et al., 2009). Moreover, the optimized transition state with the only one imaginary frequency is confirmed, then, the transition state connected with the reactant and product is verified by the method of TS confirmation.

Since the formation of C_2 oxygenates via syngas conversion usually occurs at the temperature of 500–623 K (Egbebi et al., 2010; Glezakou et al., 2012; Yin et al., 2003), all energies including the adsorption of the species and the reactions mentioned in the conversion of syngas-to- C_2 oxygenates are calculated at 525 K in our study (see details in the Part 1 of Supplementary Material).

3. Results and discussions

It is widely accepted that the mechanism of syngas conversion to produce C_2 oxygenates involves two key steps (Zhang et al.,

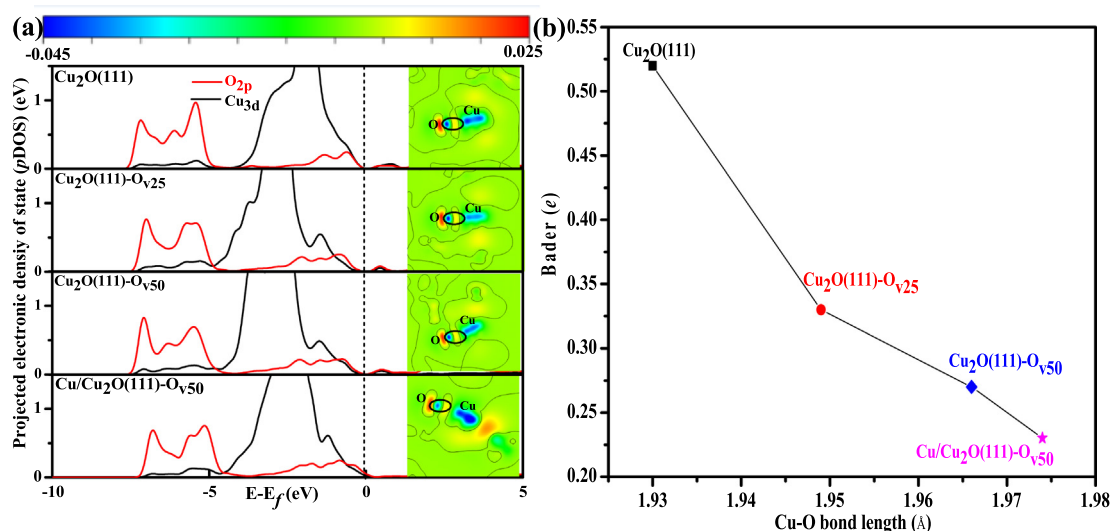


Fig. 2. (a) Projected electronic density of states (pDOS) of coordination-unsaturated Cu atom and its adjacent O atom resulting from the d - p orbital interactions, as well as the corresponding two dimensional representation of charge difference at the coordination-unsaturated Cu and its adjacent O horizontal face on the $\text{Cu}_2\text{O}(1\ 1\ 1)$, $\text{Cu}_2\text{O}(1\ 1\ 1)\text{-O}_{v25}$, $\text{Cu}_2\text{O}(1\ 1\ 1)\text{-O}_{v50}$ and $\text{Cu}/\text{Cu}_2\text{O}(1\ 1\ 1)\text{-O}_{v50}$ surfaces; (b) The relationship of the Cu–O bond length of the coordination-unsaturated Cu atom and its adjacent O with the Bader charge of the coordination-unsaturated Cu atom over the $\text{Cu}_2\text{O}(1\ 1\ 1)$, $\text{Cu}_2\text{O}(1\ 1\ 1)\text{-O}_{v25}$, $\text{Cu}_2\text{O}(1\ 1\ 1)\text{-O}_{v50}$, and $\text{Cu}/\text{Cu}_2\text{O}(1\ 1\ 1)\text{-O}_{v50}$ surfaces.

2019; Zhao et al., 2011; Schumann et al., 2018; Choi and Liu, 2009; Sun et al., 2013; Sun, 2013; Zhang et al., 2013; Zhang et al., 2013; Zheng et al., 2015); the first step is the formation of key CH_x intermediates by the C–O bond scission of CO into C, followed by successive hydrogenation; alternatively, CO hydrogenation to produce CH_xO or CH_{x-1}OH ($x = 1-3$) intermediates, followed by its C–O bond scission, in which methanol can be formed by CH_xO or CH_{x-1}OH ($x = 1-3$) hydrogenation. The second step is to produce C_2 oxygenates via the insertion of CO/CHO into the favored CH_x ($x = 1-3$) monomer, in which methane and C_2 hydrocarbons can be yielded by the hydrogenation and coupling of CH_x species, respectively. In this study, the possible reaction steps in the mechanism of syngas conversion to produce C_2 oxygenates on the Cu_2O (1 1 1), $\text{Cu}_2\text{O}(1\ 1\ 1)\text{-O}_{v25}$, $\text{Cu}_2\text{O}(1\ 1\ 1)\text{-O}_{v50}$ and $\text{Cu/Cu}_2\text{O}(1\ 1\ 1)\text{-O}_{v50}$ surfaces were investigated. Table 1 listed the activation energy barriers and reaction energies of the considered reaction steps at 525 K. In addition, the corresponding reaction steps on the Cu (1 1 1) surface have been examined in our previous studies (Sun et al., 2013; Sun, 2013).

3.1. The production of key CH_x ($x = 1-3$) intermediates

3.1.1. The adsorption of the key intermediates

The adsorption energy plays a vital role in the evaluation of the binding strength between the intermediates and the catalyst surfaces. The corresponding stable configurations (Fig. S3), adsorption free energies (Table S1) and the C–O bond lengths (Table S2) of the key intermediates (CO, CHO, CHOH, CH_2O , CH_2OH and CH_3O) involved in CO activation to produce CH_x intermediates are compared among the Cu_2O (1 1 1), $\text{Cu}_2\text{O}(1\ 1\ 1)\text{-O}_{v25}$, $\text{Cu}_2\text{O}(1\ 1\ 1)\text{-O}_{v50}$ and $\text{Cu/Cu}_2\text{O}(1\ 1\ 1)\text{-O}_{v50}$ surfaces. The results show that the most stable adsorption sites are the coordination-unsaturated Cu^+ site or the $\text{Cu}^{\delta+}$ ($0 < \delta < 1$) sites consisted by the original coordination-unsaturated Cu atom and its surrounding coordination-saturated Cu atom over the four surfaces, namely, the coordination-unsaturated Cu atoms can be considered as the active site, which is also supported by Huang (2016) and Yang et al. (2018) for the adsorption of CO_2 and CO on the $\text{Cu}_2\text{O}(1\ 1\ 1)$ surface that the coordination-unsaturated Cu is also the active sites due to the strong adsorption ability.

As presented in Fig. 3, the length of C–O bond in the CH_xO ($x = 0-3$) and CH_xOH ($x = 1,2$) intermediates over the $\text{Cu}_2\text{O}(1\ 1\ 1)\text{-O}_{v25}$, $\text{Cu}_2\text{O}(1\ 1\ 1)\text{-O}_{v50}$ and $\text{Cu/Cu}_2\text{O}(1\ 1\ 1)\text{-O}_{v50}$ surfaces are longer than those over the $\text{Cu}_2\text{O}(1\ 1\ 1)$ surface, namely, the easier scission of C–O bond in CH_xO ($x = 0-3$) and CH_xOH ($x = 1,2$) species on these metastable surfaces potentially promote the formation of key CH_x intermediate, especially, the $\text{Cu/Cu}_2\text{O}(1\ 1\ 1)\text{-O}_{v50}$ surface with Cu/ Cu_2O interface.

3.1.2. CO initial activation

The initial activation of CO involves direct CO dissociation and CO hydrogenation to CHO or COH. Since the occurrence of direct CO dissociation on the Cu (Sun et al., 2013; Sun, 2013; Zhang et al., 2013; Zhang et al., 2013; Zheng et al., 2015) and Rh (Zhao et al., 2011; Choi and Liu, 2009; Kapur et al., 2010; Yang et al., 2016) catalysts is difficult, moreover, the (1 1 1) (Sun et al., 2013; Sun, 2013); (1 1 0) (Sun, 2013; Zhang et al., 2013) and (1 0 0) (Sun, 2013; Zheng et al., 2015) surfaces of Cu catalysts prefer to catalyze CO hydrogenation to produce CHO instead of COH; thus, in this study, only the hydrogen-assisted CO to produce CHO is investigated for CO initial activation on the $\text{Cu}_2\text{O}(1\ 1\ 1)$, $\text{Cu}_2\text{O}(1\ 1\ 1)\text{-O}_{v25}$, $\text{Cu}_2\text{O}(1\ 1\ 1)\text{-O}_{v50}$ and $\text{Cu/Cu}_2\text{O}(1\ 1\ 1)\text{-O}_{v50}$ surfaces. As illustrated in Fig. 4a, the $\text{Cu}_2\text{O}(1\ 1\ 1)$ surface with the Cu^+ sites has better catalytic activity for CO initial activation compared to the Cu^0 sites (Sun et al., 2013) (86.2 vs. 105.8 $\text{kJ}\cdot\text{mol}^{-1}$). Meanwhile, the interface $\text{Cu}^{\delta+}$ ($0 < \delta < 1$) site of $\text{Cu/Cu}_2\text{O}(1\ 1\ 1)\text{-O}_{v50}$ surface is more favorable for CO initial activation in kinetics than the $\text{Cu}^{\delta+}$ ($0 < \delta < 1$) site of $\text{Cu}_2\text{O}(1\ 1\ 1)\text{-O}_{v25}$ and $\text{Cu}_2\text{O}(1\ 1\ 1)\text{-O}_{v50}$ surfaces (78.0 vs. 124.0 and 100.6 $\text{kJ}\cdot\text{mol}^{-1}$). Further, CO initial activation at the interface $\text{Cu}^{\delta+}$ ($0 < \delta < 1$) site of $\text{Cu/Cu}_2\text{O}(1\ 1\ 1)\text{-O}_{v50}$ surface is more favored in kinetics than that at the Cu^+ and Cu^0 sites.

As mentioned above, the interface $\text{Cu}^{\delta+}$ ($0 < \delta < 1$) site is more favorable CO initial activation than the Cu^+ site, the analysis of pDOS on the $\text{Cu/Cu}_2\text{O}(1\ 1\ 1)\text{-O}_{v50}$ and $\text{Cu}_2\text{O}(1\ 1\ 1)$ surfaces was carried out to further illustrate the correlations of the catalytic performance with the electronic properties, as shown in Fig. 4b, CO is inclined to bind with the interface Cu–Cu bridge site of $\text{Cu/Cu}_2\text{O}(1\ 1\ 1)\text{-O}_{v50}$ surface, whereas CO is adsorbed at the top coordination-unsaturated Cu site of $\text{Cu}_2\text{O}(1\ 1\ 1)$ surface, as a result, the difference of CO adsorption sites leads to different hybridiza-

Table 1

Calculated activation energy barrier (ΔG_a) and reaction energy (ΔG) of the elementary reactions involving in the formation of C_2 oxygenates from syngas over the $\text{Cu}_2\text{O}(1\ 1\ 1)$, $\text{Cu}_2\text{O}(1\ 1\ 1)\text{-O}_{v25}$, $\text{Cu}_2\text{O}(1\ 1\ 1)\text{-O}_{v50}$ and $\text{Cu/Cu}_2\text{O}(1\ 1\ 1)\text{-O}_{v50}$ surfaces at 525 K, respectively.

Reactions*	$\Delta G_a(\Delta G)/\text{kJ}\cdot\text{mol}^{-1}$	$\text{Cu}^{\delta+}$ ($0 < \delta < 1$) sites			
		Cu ⁺ site			
		$\text{Cu}_2\text{O}(1\ 1\ 1)$	$\text{Cu}_2\text{O}(1\ 1\ 1)\text{-O}_{v25}$	$\text{Cu}_2\text{O}(1\ 1\ 1)\text{-O}_{v50}$	$\text{Cu/Cu}_2\text{O}(1\ 1\ 1)\text{-O}_{v50}$
Rx-1	$\text{CO} + \text{H} \rightarrow \text{CHO}$	86.2(−0.5)	124.0(48.1)	100.6(46.0)	78.0(3.4)
Rx-2	$\text{CHO} \rightarrow \text{CH} + \text{O}$	387.5(315.4)	299.4(88.4)	258.7(121.0)	215.8(42.1)
Rx-3	$\text{CHO} + \text{H} \rightarrow \text{CHOH}$	78.4(−56.8)	66.1(25.4)	82.3(40.5)	125.9(36.0)
Rx-4	$\text{CHOH} \rightarrow \text{CH} + \text{OH}$	249.4(184.4)	185.3(−89.8)	203.5(103.4)	220.1(98.3)
Rx-5	$\text{CHO} + \text{H} \rightarrow \text{CH}_2\text{O}$	8.6(−67.5)	60.6(−29.5)	84.0(−17.9)	79.9(−17.7)
Rx-6	$\text{CH}_2\text{O} \rightarrow \text{CH}_2 + \text{O}$	262.4(234.5)	260.2(45.6)	106.7(−37.2)	121.5(−36.5)
Rx-7	$\text{CH}_2\text{O} + \text{H} \rightarrow \text{CH}_2\text{OH}$	11.6(−69.0)	127.7(−21.5)	126.9(−8.3)	114.5(−23.8)
Rx-8	$\text{CHOH} + \text{H} \rightarrow \text{CH}_2\text{OH}$	5.7(−97.1)	65.1(−52.8)	37.1(−65.6)	16.3(−68.3)
Rx-9	$\text{CH}_2\text{OH} \rightarrow \text{CH}_2 + \text{OH}$	176.2(114.3)	133.5(−29.2)	176.1(14.0)	191.4(−17.2)
Rx-10	$\text{CH}_2\text{O} + \text{H} \rightarrow \text{CH}_3\text{O}$	8.8(−103.8)	9.1(−112.7)	179.9(−31.9)	209.0(−11.3)
Rx-11	$\text{CH}_3\text{O} \rightarrow \text{CH}_3 + \text{O}$	221.8(152.8)	175.9(−60.9)	171.1(−89.9)	231.7(−145.6)
Rx-12	$\text{CH}_3\text{O} + \text{H} \rightarrow \text{CH}_3\text{OH}$	13.3(−133.5)	36.7(−94.9)	44.3(−9.7)	85.8(3.1)
Rx-13	$\text{CH}_2\text{OH} + \text{H} \rightarrow \text{CH}_3\text{OH}$	8.2(−149.8)	46.5(−98.3)	57.4(−60.9)	59.6(−57.8)
Rx-14	$\text{CH}_2 + \text{H} \rightarrow \text{CH}_3$	97.1(−188.6)	126.5(−67.1)	38.9(−50.7)	53.9(−45.6)
Rx-15	$\text{CH}_3 + \text{H} \rightarrow \text{CH}_4$	101.6(−49.0)	35.5(−54.2)	94.1(−66.8)	92.2(−67.0)
Rx-16	$\text{CH}_2 + \text{CH}_2 \rightarrow \text{C}_2\text{H}_4$	135.0(−312.6)	96.2(−254.6)	103.5(−44.1)	107.7(−42.1)
Rx-17	$\text{CO} + \text{CH}_2 \rightarrow \text{CH}_2\text{CO}$	90.6(−142.4)	136.5(−36.4)	92.5(−18.3)	90.9(−24.6)
Rx-18	$\text{CHO} + \text{CH}_2 \rightarrow \text{CH}_2\text{CHO}$	70.0(−152.8)	82.9(−108.7)	16.8(−142.7)	20.0(−148.9)

* It is noted that the values of \times is 1–4 corresponding to the $\text{Cu}_2\text{O}(1\ 1\ 1)$, $\text{Cu}_2\text{O}(1\ 1\ 1)\text{-O}_{v25}$, $\text{Cu}_2\text{O}(1\ 1\ 1)\text{-O}_{v50}$ and $\text{Cu/Cu}_2\text{O}(1\ 1\ 1)\text{-O}_{v50}$ surfaces, respectively.

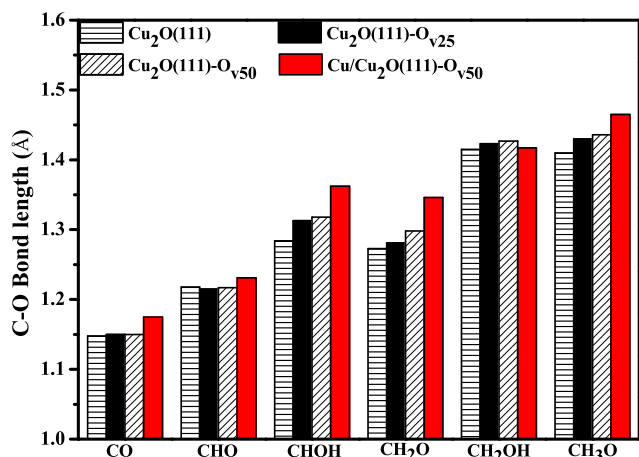


Fig. 3. The C–O bond length of key intermediates CO, CHO, CHOH, CH₂OH, CH₃O and CH₃OH on the Cu₂O(1 1 1), Cu₂O(1 1 1)-O_{v25}, Cu₂O(1 1 1)-O_{v50} and Cu/Cu₂O(1 1 1)-O_{v50} surfaces, respectively.

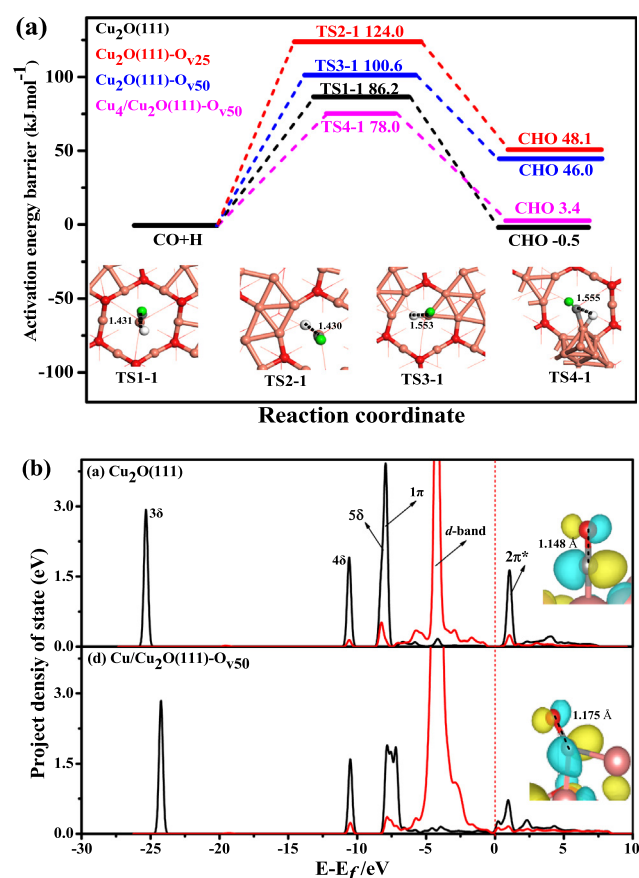


Fig. 4. (a) The potential energy diagram of CO initial activation together with the transition state on the Cu₂O(1 1 1), Cu₂O(1 1 1)-O_{v25}, Cu₂O(1 1 1)-O_{v50} and Cu/Cu₂O(1 1 1)-O_{v50} surfaces, respectively; (b) Projected electronic density of states (pDOS) of CO and its adsorption Cu sites on the Cu₂O(1 1 1) and Cu/Cu₂O(1 1 1)-O_{v50} surfaces. Bond lengths are in Å. The orange and red balls represent Cu and O atom of the catalyst surfaces; the gray, white and green balls are the C, H and O atoms participating into the reaction. (For interpretation of the references to colour in this figure legend, the reader is referred to the web version of this article.)

tion degree between the anti-bond orbital of CO and the *d*-orbital of Cu/Cu₂O(1 1 1)-O_{v50} interface site, and the Cu/Cu₂O(1 1 1)-O_{v50} surface is obviously stronger than that of Cu₂O(1 1 1) surface, that is, the amount of electrons transferred from the metal *d*-or-

bit to the anti-bond orbital of adsorbed CO increases, resulting in the C–O bond weakening of CO at the interface site of Cu/Cu₂O(1 1 1)-O_{v50} surface (Sung and Hoffmann, 1985; Hu et al., 1995), which is in good agreement with our kinetic results.

3.1.3. The formation of CH_x intermediate and CH₃OH

Based on above analysis, the initial activation of CO dominantly lead to CHO species, beginning with the CHO and CO + H species, according to previous studies (Sun et al., 2016; Yue et al., 2014; Gupta et al., 2011); the possible formation routes of CH_x intermediate and methanol are considered, Fig. 5 shows the energy profile for the optimal formation routes of CH_x (*x* = 1–3) and CH₃OH (see details in Figs. S4–S9).

On the Cu₂O(1 1 1) surface, as presented in Fig. 5a, the dominant route of CH formation is CHO + H → CHOH → CH + OH with the overall energy barrier of 192.6 kJ·mol⁻¹ and reaction energy of 127.6 kJ·mol⁻¹. The route of CHO + H → CH₂O + H → CH₂OH → CH₂ + OH mainly produce CH₂ with the overall energy barrier of 39.7 kJ·mol⁻¹ and reaction energy of –22.2 kJ·mol⁻¹. Only the route of CHO + H → CH₂O + H → CH₃O → CH₃ + O contributes to CH₃ formation with the overall energy barrier of 50.5 kJ·mol⁻¹. Meanwhile, due to the close activation energy barriers of CH₂O + H → CH₃O and CH₂O + H → CH₂OH (8.8 and 11.6 kJ·mol⁻¹), methanol formation is competitive between the routes of CH₂O + H → C H₂O + H → CH₃OH and CH₂O + H → CH₂OH + H → CH₃OH corresponding to the same overall energy barrier of 8.6 kJ·mol⁻¹, which are exothermic by 286.3 and 304.8 kJ·mol⁻¹, respectively. As a result, CH₂ monomer is preferentially formed in kinetics among the CH_x (*x* = 1–3) species (39.7 vs. 192.6, 50.5 kJ·mol⁻¹). Moreover, methanol formation is also kinetically preferred in comparison with CH_x (*x* = 1–3) formation (8.6 vs. 192.6, 39.7 and 50.5 kJ·mol⁻¹), that is, the Cu₂O(1 1 1) surface dominantly contribute to the formation of methanol instead of CH_x intermediates.

Similar to the Cu₂O(1 1 1) surface, as presented in Fig. 5b–d, on the Cu₂O(1 1 1)-O_{v25} surface, the overall energy barriers for the formation of CH, CH₂, CH₃ and CH₃OH correspond to 210.7, 106.1, 60.6 and 60.6 kJ·mol⁻¹, respectively; CH₃O → CH₃ + O is very difficult in kinetics compared to CH₃O + H → CH₃OH (175.9 vs. 36.7 kJ·mol⁻¹), hence, the Cu₂O(1 1 1)-O_{v25} surface is more favorable for methanol formation instead of CH_x intermediates. Interestingly, both Cu₂O(1 1 1)-O_{v50} and Cu/Cu₂O(1 1 1)-O_{v50} surfaces are favorable for the formation of the most preferred CH₂ intermediate in kinetics (88.8 and 103.8 kJ·mol⁻¹), which becomes energetically competitive with methanol formation (82.3 and 96.8 kJ·mol⁻¹).

3.2. The effect of Cu^{δ+} (0 ≤ δ ≤ 1) sites on the formation of preferred CH_x monomer

As presented in Fig. 6a, the preferred CH_x monomer on the Cu₂O(1 1 1) surface is CH₂ formed by the C–O bond breakage of CH₂OH intermediate; moreover, CH₃OH formation is much easier in kinetics than CH₂ formation (8.6 vs. 39.7 kJ·mol⁻¹), thus, the Cu⁺ sites dominantly contribute to CH₃OH formation. For the Cu^{δ+} (0 < δ < 1) sites, on the Cu₂O(1 1 1)-O_{v25} surface, CH₂ is also the preferred CH_x monomer arisen from the breakage of C–O bond in CH₂OH species, while CH₃OH formation is preferred in kinetics compared to CH₂ formation. On the Cu₂O(1 1 1)-O_{v50} and Cu/Cu₂O(1 1 1)-O_{v50} surfaces, CH₂ intermediate is still the preferred CH_x monomer formed by the breakage of C–O bond in CH₂O species; meanwhile, CH₃OH formation is energetically competitive with CH₂ formation. Further, syngas conversion on the (1 1 1) (Sun et al., 2013; Sun, 2013); (2 1 1) (Zhang et al., 2013); (1 1 0) (Sun, 2013; Zhang et al., 2013) and (1 0 0) (Sun, 2013; Zheng et al., 2015) surfaces of Cu catalyst acted as the Cu⁰ sites showed that the preferred CH_x species is CH₂ or CH₃; while CH₃OH formation is kinetically preferred in comparison with CH_x (*x* = 1–3) formation. Therefore,

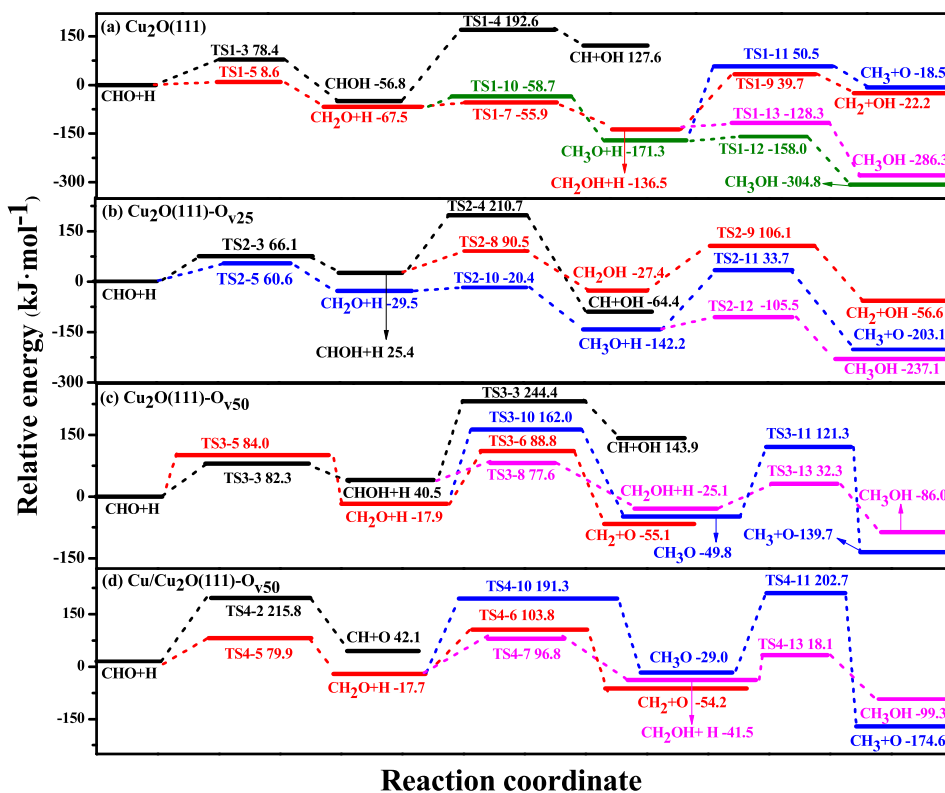


Fig. 5. The potential energy profiles for the most favorable route of CH, CH₂, CH₃ and CH₃OH formation on the (a) Cu₂O(1 1 1), (b) Cu₂O(1 1 1)-O_{v25}, (c) Cu₂O(1 1 1)-O_{v50} and (d) Cu/Cu₂O(1 1 1)-O_{v50} surfaces; the corresponding structures of the initial states, transition states and final states are presented in Figs. S4–S9.

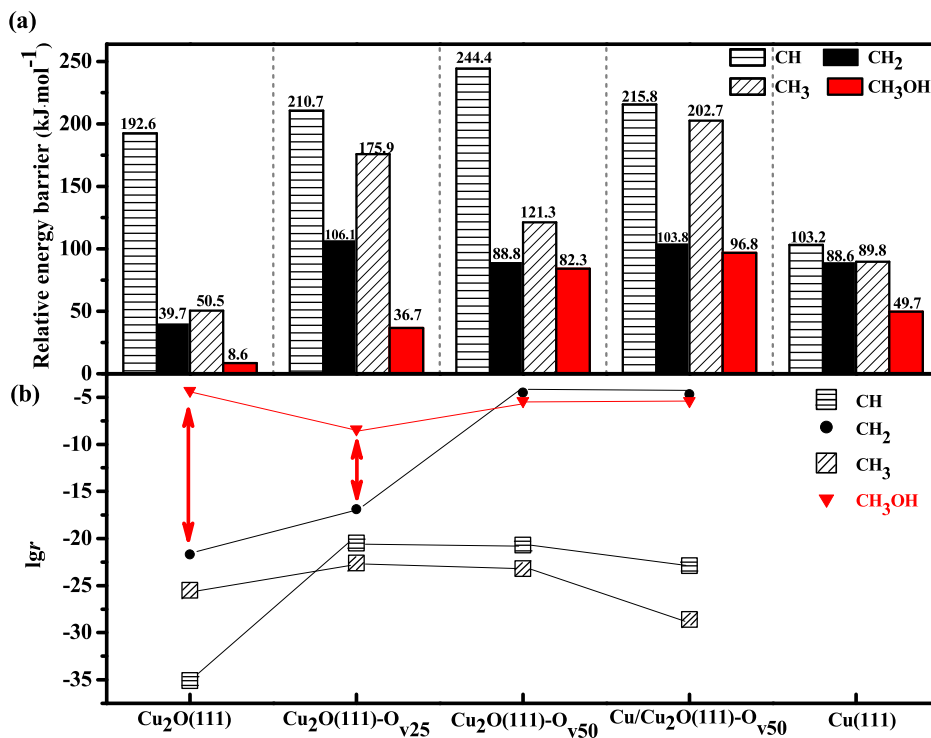


Fig. 6. (a) The relative energy barrier for the most favorable routes of CH_x (x = 1–3) and CH₃OH formation with respect to the CHO + H species on the Cu₂O(1 1 1), Cu₂O(1 1 1)-O_{v25}, Cu₂O(1 1 1)-O_{v50}, Cu/Cu₂O(1 1 1)-O_{v50} and Cu(1 1 1) (Sun et al., 2013; Sun, 2013) surfaces, (b) the formation rates of CH_x (x = 1–3) intermediate and CH₃OH over the Cu₂O(1 1 1), Cu₂O(1 1 1)-O_{v25}, Cu₂O(1 1 1)-O_{v50} and Cu/Cu₂O(1 1 1)-O_{v50} surfaces at 525 K.

compared to the Cu₂O(1 1 1), Cu(1 1 1) and Cu₂O(1 1 1)-O_{v25} surfaces, both Cu₂O(1 1 1)-O_{v50} and Cu/Cu₂O(1 1 1)-O_{v50} surfaces significantly favored the production of the preferred CH₂ monomer and suppress CH₃OH formation.

To gain further insight into the effect of Cu^{δ+} (0 ≤ δ ≤ 1) sites on the formation of preferred CH_x monomer under the typical experimental conditions, the microkinetic modeling calculations (Choi and Liu, 2009; Liu et al., 2017; Shetty et al., 2010) have been carried out at a typical operating condition (P_{CO} = 4 atm, P_{H₂} = 8 atm, T = 525 K) for the formation of CH_x (x = 1–3) from syngas over the Cu₂O(1 1 1), Cu₂O(1 1 1)-O_{v25}, Cu₂O(1 1 1)-O_{v50} and Cu/Cu₂O(1 1 1)-O_{v50} surfaces, which will allow us to obtain the activity and selectivity (see details in the Part 7 of Supplementary Material). The surface coverage of the mentioned species, the formation rates of CH_x intermediate and methanol are presented in Table 2. As indicated in Fig. 6b, the formation rate of CH₂ species is much faster than those of CH and CH₃ species on the Cu₂O(1 1 1), Cu₂O(1 1 1)-O_{v25}, Cu₂O(1 1 1)-O_{v50} and Cu/Cu₂O(1 1 1)-O_{v50} surfaces, thus, the CH₂ species is the preferred CH_x monomer. Meanwhile, the activity order of the preferred CH₂ monomer production is Cu/Cu₂O(1 1 1)-O_{v50} ≈ Cu₂O(1 1 1)-O_{v50} > Cu₂O(1 1 1)-O_{v25} > Cu₂O(1 1 1), namely, compared to the Cu⁺ sites over the Cu₂O(1 1 1) surface, the Cu^{δ+} (0 < δ < 1) sites over the Cu₂O(1 1 1)-O_{v25}, Cu₂O(1 1 1)-O_{v50} and Cu/Cu₂O(1 1 1)-O_{v50} surfaces significantly enhanced the catalytic activity of CO activation and conversion to produce the preferred CH₂ monomer, especially, the moderate valence state (0.43 and 0.51) Cu^{δ+} (0 < δ < 1) sites over the Cu/Cu₂O(1 1 1)-O_{v50} and Cu₂O(1 1 1)-O_{v50} surfaces. Further, the relative selectivity of the preferred CH_x species along with methanol formation is defined as $S_{CH_x} = \frac{r_{CH_x}}{(r_{CH_x} + r_{CH_3OH})} \times 100\%$, the selectivity of the preferred CH₂ monomer on the Cu₂O(1 1 1), Cu₂O(1 1 1)-O_{v25}, Cu₂O(1 1 1)-O_{v50} and Cu/Cu₂O(1 1 1)-O_{v50} surfaces are 0%, 0%, 87.5% and 83.9%, respectively. Thus, compared to the Cu⁺ and Cu⁰ sites, the moderate valence state Cu^{δ+} (δ = 0.43 and 0.51) sites can highly-active and highly-selective catalyze CO activation to form the preferred CH₂ monomer, which also agree with our DFT results that the CH₂ monomer is preferentially formed over the Cu₂O(1 1 1)-O_{v50} and Cu/Cu₂O(1 1 1)-O_{v50}.

On the other hand, since the moderate valence state Cu^{δ+} (δ = 0.43 and 0.51) sites at 525 K can highly-active and highly-selective catalyze CO activation to form the preferred CH₂ monomer, the effect of reaction temperature on the catalytic activity and selectivity of CH_x formation over the Cu₂O(1 1 1)-O_{v50} and Cu/Cu₂O(1 1 1)-O_{v50} surfaces was considered. As shown in Fig. 7(a) and (b), on the Cu₂O(1 1 1)-O_{v50} and Cu/Cu₂O(1 1 1)-O_{v50} surfaces, the formation rate of CH_x (x = 1–3) and CH₃OH increases obviously when the reaction temperature increases from 450 K to 700 K, but CH₂ spe-

cies is still the preferred CH_x monomer. Meanwhile, the effect of reaction temperature on the relative selectivity of the preferred CH_x species along with CH₃OH formation was further considered; on the Cu₂O(1 1 1)-O_{v50} surface, as presented in Fig. 7(c), the selectivity of the most favored monomer CH₂ firstly increases and then decreases with the reaction temperature increasing from 450 K to 700 K, especially, when the reaction temperature is higher than 600 K, the selectivity of CH₂ decreases sharply; when the temperature is at 525 K, it has the best CH₂ selectivity; however, on the Cu/Cu₂O(1 1 1)-O_{v50} surface, as presented in Fig. 7(d), the selectivity of the most favored monomer CH₂ decreases with the reaction temperature increasing from 450 K to 700 K, namely, the low temperature is in favor of the selectivity of the most favored monomer CH₂ on the Cu/Cu₂O(1 1 1)-O_{v50} surface.

Based on above DFT calculations and microkinetic modeling on the Cu⁺ and Cu^{δ+} (0 < δ < 1) sites, taking previous studies over the Cu⁰ sites into consideration (Sun et al., 2013; Sun, 2013; Zhang et al., 2013; Zhang et al., 2013; Zheng et al., 2015), we can obtain that CH₂ species is the preferred CH_x monomer on the Cu^δ (0 ≤ δ ≤ 1) sites; moreover, when the Cu⁺ and Cu⁰ sites corresponding to higher and lower valence state are acted as the active site in the process of syngas conversion, the production of methanol is more advantageous in kinetics than that of CH_x; whereas the moderate valence state Cu^{δ+} (δ = 0.43 and 0.51) sites are acted as the active site, the formation of the preferred CH₂ intermediate is more conducive than methanol formation, namely, in the reducing atmosphere of syngas conversion, the Cu catalyst prepared in experiment should focus on the metastable Cu^{δ+} (0 < δ < 1) surface with the moderate valence state Cu^{δ+} (δ = 0.43 and 0.51) sites, which can highly-active and highly-selective catalyze syngas conversion to produce the preferred CH₂ monomer instead of methanol.

Further, our results show that although the surface geometrical structure of Cu₂O(1 1 1)-O_{v25} is similar to that of Cu₂O(1 1 1)-O_{v50}, Cu₂O(1 1 1)-O_{v25} surface exhibits high selectivity of methanol instead of CH_x intermediate and C₂ oxygenates, while Cu₂O(1 1 1)-O_{v50} surface can highly-active and highly-selective catalyze syngas conversion to produce the preferred CH₂ monomer instead of methanol. Meanwhile, the surface geometrical structure of Cu₂O(1 1 1)-O_{v50} is quite different from that of Cu/Cu₂O(1 1 1)-O_{v50}, however, the adsorption configuration of the key species (CO, CHO, CHOH, CH₂O, CH₂OH and CH₃O) involved in CO activation to produce CH_x intermediates are similar between Cu₂O(1 1 1)-O_{v50} and Cu/Cu₂O(1 1 1)-O_{v50} surfaces (See Part 4 of Supplementary Material), moreover, both Cu₂O(1 1 1)-O_{v50} and Cu/Cu₂O(1 1 1)-O_{v50} surfaces can highly-active and highly-selective catalyze CO activation to form the preferred CH₂ monomer and C₂

Table 2
The surface coverage of all species, the formation rates of CH_x intermediate and methanol over the Cu₂O(1 1 1), Cu₂O(1 1 1)-O_{v25}, Cu₂O(1 1 1)-O_{v50}, and Cu/Cu₂O(1 1 1)-O_{v50} at 525 K.

Parameters		Cu ₂ O(1 1 1)	Cu ₂ O(1 1 1)-O _{v25}	Cu ₂ O(1 1 1)-O _{v50}	Cu/Cu ₂ O(1 1 1)-O _{v50}
Coverage	θ _{CO}	1.00 × 10 ⁰	1.00 × 10 ⁰	9.97 × 10 ⁻¹	8.76 × 10 ⁻¹
	θ _H	3.67 × 10 ⁻⁷	2.47 × 10 ⁻⁷	7.38 × 10 ⁻⁶	1.32 × 10 ⁻⁷
	θ _{CHO}	2.28 × 10 ⁻¹⁰	7.15 × 10 ⁻⁹	3.20 × 10 ⁻⁵	4.60 × 10 ⁻⁹
	θ _{CHOH}	3.64 × 10 ⁻¹⁸	3.88 × 10 ⁻⁹	4.29 × 10 ⁻¹⁰	2.15 × 10 ⁻¹⁶
	θ _{CH₂O}	2.17 × 10 ⁻¹¹	1.47 × 10 ⁻¹⁵	3.46 × 10 ⁻⁸	1.24 × 10 ⁻¹
	θ _{CH₂OH}	9.28 × 10 ⁻¹³	9.55 × 10 ⁻¹¹	1.05 × 10 ⁻⁸	1.54 × 10 ⁻⁷
	θ _{CH₃O}	2.01 × 10 ⁻¹⁰	6.34 × 10 ⁻¹³	7.16 × 10 ⁻¹⁶	1.07 × 10 ⁻¹⁴
	θ*	3.74 × 10 ⁻⁶	1.95 × 10 ⁻⁶	3.89 × 10 ⁻⁴	3.16 × 10 ⁻⁵
	Formation rates (s ⁻¹)	r _{CH}	8.05 × 10 ⁻³⁶	3.28 × 10 ⁻²¹	2.00 × 10 ⁻²¹
r _{CH₂}		1.85 × 10 ⁻²²	1.36 × 10 ⁻¹⁷	2.90 × 10 ⁻⁵	2.00 × 10 ⁻⁵
r _{CH₃}		3.00 × 10 ⁻²⁶	2.67 × 10 ⁻²³	6.44 × 10 ⁻²⁴	2.56 × 10 ⁻²⁹
r _{CH₃OH}		5.26 × 10 ⁻⁵	4.68 × 10 ⁻⁹	4.13 × 10 ⁻⁶	3.84 × 10 ⁻⁶
Relative selectivity (%)	S _{CH₂}	0	0	87.5	83.9

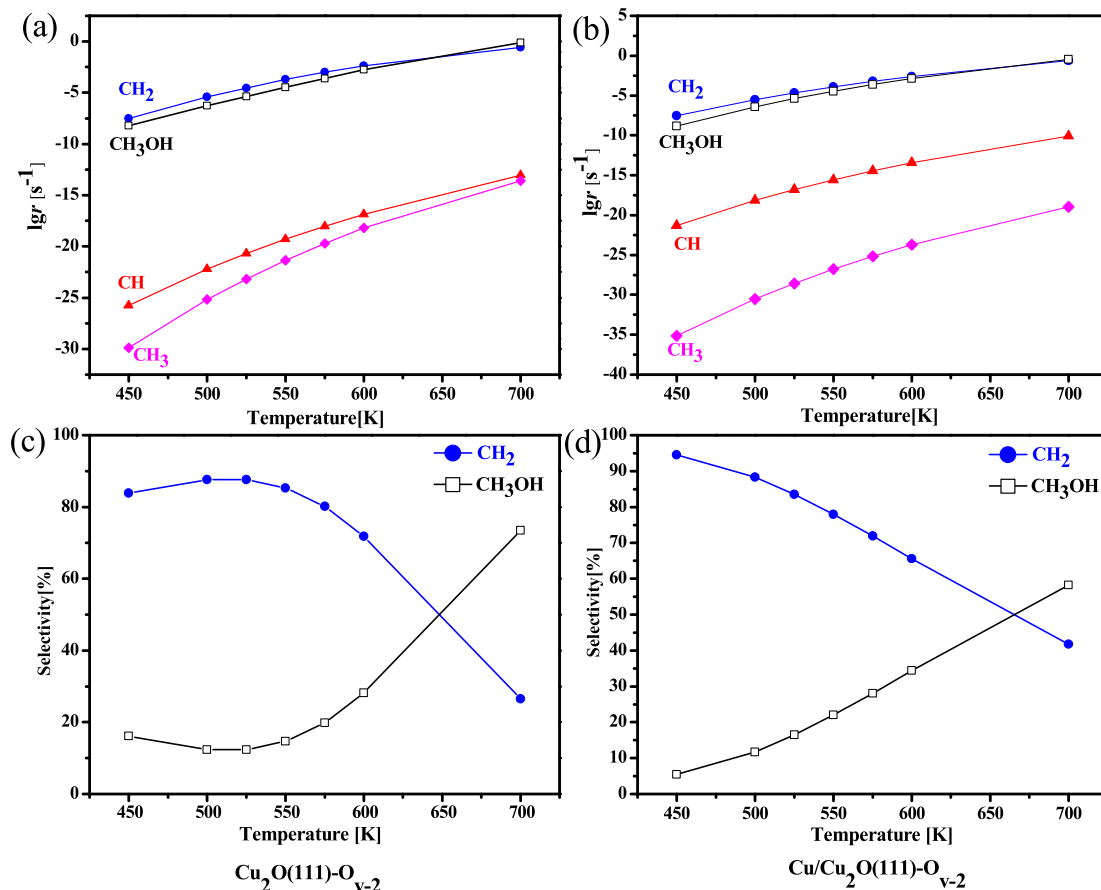


Fig. 7. The trend of the formation rates of CH_x ($x = 1-3$) intermediate and CH_3OH over the (a) $\text{Cu}_2\text{O}(1\ 1\ 1)\text{-O}_{v50}$ and (b) $\text{Cu/Cu}_2\text{O}(1\ 1\ 1)\text{-O}_{v50}$ surfaces with temperature; The trend of relative selectivity of the favored CH_2 intermediate and CH_3OH over the (c) $\text{Cu}_2\text{O}(1\ 1\ 1)\text{-O}_{v50}$ and (d) $\text{Cu/Cu}_2\text{O}(1\ 1\ 1)\text{-O}_{v50}$ surfaces with the change of the temperature.

oxygenates. On the other hand, the catalytic activity of transition metals is closely related to their corresponding d -electrons and/or empty d -orbitals (Carter, 2008; Zhang et al., 2017; Hammer and Nørskov, 1995). As presented in Fig. 8; the d -band center of the moderate valence state $\text{Cu}^{\delta+}$ ($\delta = 0.43$ and 0.51) sites (Cu_2O

$(1\ 1\ 1)\text{-O}_{v50}$ and $\text{Cu/Cu}_2\text{O}(1\ 1\ 1)\text{-O}_{v50}$ surfaces correspond to -1.79 and -1.75 eV) are closer to the Fermi level in comparison to the Cu^+ and Cu^0 sites ($\text{Cu}_2\text{O}(1\ 1\ 1)$ and $\text{Cu}(1\ 1\ 1)$ surfaces correspond to -2.28 and -2.47 eV), namely, the closer the d -band center of $\text{Cu}^{\delta+}$ ($0 \leq \delta \leq 1$) sites to the Fermi level is, the more active the formation of the preferred CH_2 monomer is, which well explained our results obtained by the DFT calculations and microkinetic modeling. Above these results show that the catalytic performance of $\text{Cu}^{\delta+}$ ($0 \leq \delta \leq 1$) active sites is dominantly affected by the electronic effect instead of the geometry effect.

3.3. The formation of C_2 oxygenates

Lots of recent studies (Choi and Liu, 2009; Kapur et al., 2010; Yang et al., 2016; Liu et al., 2017; Sun, 2013; Zhang et al., 2013; Zhang et al., 2013; Zheng et al., 2015) showed that once CH_x ($x = 1-3$) species were produced, the reactions including the hydrogenation of CH_x to CH_4 , $\text{CH}_x\text{-CH}_x$ coupling to C_2 hydrocarbons and the insertion of CHO/CO into CH_x to C_2 oxygenates may occur, in which the formation of C_2 hydrocarbons and CH_4 reduce the selectivity and production of C_2 oxygenates (Zhang et al., 2019; Choi and Liu, 2009; Egbebi et al., 2010; Glezakou et al., 2012; Sun, 2013; Zhang et al., 2013; Zhang et al., 2013; Zheng et al., 2015). As mentioned above, since the preferred CH_x species is CH_2 monomer on the $\text{Cu}_2\text{O}(1\ 1\ 1)$, $\text{Cu}(1\ 1\ 1)$, $\text{Cu}_2\text{O}(1\ 1\ 1)\text{-O}_{v25}$, $\text{Cu}_2\text{O}(1\ 1\ 1)\text{-O}_{v50}$ and $\text{Cu/Cu}_2\text{O}(1\ 1\ 1)\text{-O}_{v50}$ surfaces, starting with the preferred CH_2 monomer, the related reactions of CH_2 monomer are examined.

Fig. 9 displays the overall energy barriers for the related reactions of CH_2 species on the five surfaces (see details in Figs. S10 and S11). On the $\text{Cu}_2\text{O}(1\ 1\ 1)$ surface, the formations of CH_4 ,

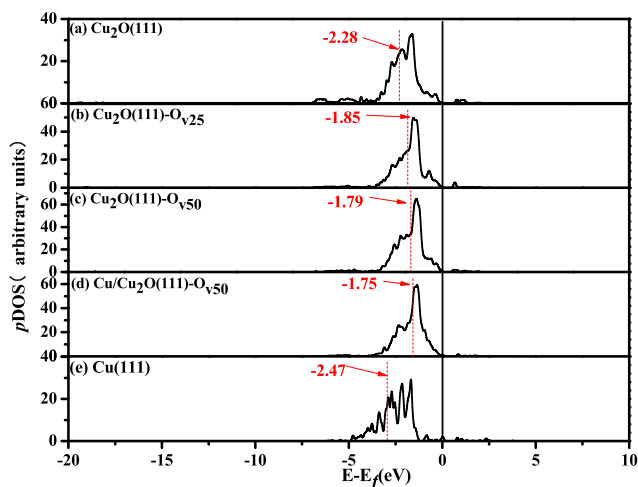


Fig. 8. Projected density of states (pDOS) plots of the d -orbitals is corresponds to coordination-unsaturated Cu atom and the surrounding coordination-saturated Cu atom on the (a) $\text{Cu}_2\text{O}(1\ 1\ 1)$, (b) $\text{Cu}_2\text{O}(1\ 1\ 1)\text{-O}_{v25}$, (c) $\text{Cu}_2\text{O}(1\ 1\ 1)\text{-O}_{v50}$, (d) $\text{Cu/Cu}_2\text{O}(1\ 1\ 1)\text{-O}_{v50}$ and (e) $\text{Cu}(1\ 1\ 1)$ surfaces. The vertical red dotted lines represent the location of d -band center, and the vertical black solid lines indicate Fermi energy level. (For interpretation of the references to colour in this figure legend, the reader is referred to the web version of this article.)

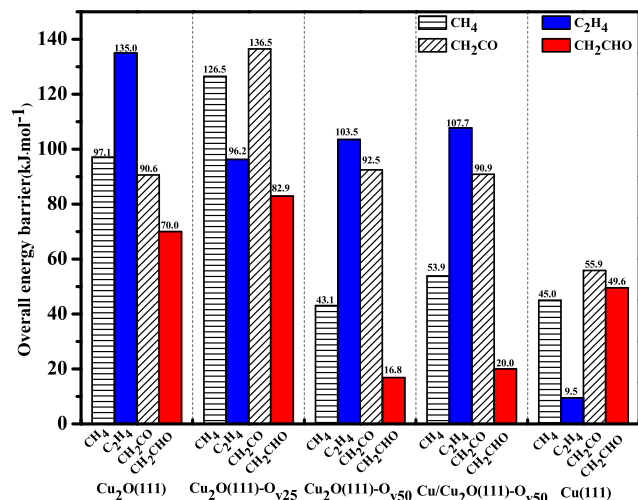


Fig. 9. The overall energy barriers for the reactions related to CH₂ species on the Cu₂O(1 1 1), Cu₂O(1 1 1)-O_{v25}, Cu₂O(1 1 1)-O_{v50}, Cu/Cu₂O(1 1 1)-O_{v50} and Cu(1 1 1) (Sun, 2013) surfaces at 525 K.

C₂H₄, CH₂CO and CH₂CHO have the overall energy barriers of 97.1, 135.0, 90.6 and 70.0 kJ.mol⁻¹, respectively, namely, the C₂ oxygenates CH₂CHO is preferentially formed. Similar to the Cu₂O(1 1 1) surface, the Cu₂O(1 1 1)-O_{v25}, Cu₂O(1 1 1)-O_{v50} and Cu/Cu₂O(1 1 1)-O_{v50} surfaces are also in favor of CH₂CHO formation by CHO reaction with CH₂ in kinetics (82.9, 16.8 and 20.0 kJ.mol⁻¹). However, on the Cu(1 1 1) surface acted as the Cu⁰ sites (Sun et al., 2013; Sun, 2013); the preferred CH₂ or CH₃ monomer is inclined to C₂H₄ formation by CH₂ self-coupling or CH₄ formation by CH₃ hydrogenation, respectively. Thus, the Cu₂O(1 1 1), Cu₂O(1 1 1)-O_{v25}, Cu₂O(1 1 1)-O_{v50} and Cu/Cu₂O(1 1 1)-O_{v50} surfaces not only exhibit excellent selectivity toward C₂ oxygenates, but also suppress the production of CH₄ and C₂ hydrocarbons.

3.4. The effect of Cu^{δ+}(0 ≤ δ ≤ 1) sites on the formation of C₂ oxygenates

As described above, the Cu⁺ and Cu^{δ+}(0 < δ < 1) sites is highly-selective for C₂ oxygenates formation; whereas the Cu⁰ sites exhibits preferable selectivity toward methane and C₂ hydrocarbons instead of C₂ oxygenates (Sun et al., 2013; Sun, 2013). Thus, once the preferred CH₂ species was generated, compared to the Cu⁰ sites, both Cu⁺ and Cu^{δ+}(0 < δ < 1) sites essentially improve the selectivity of C₂ oxygenates CH₂CHO.

The selectivity of C₂ oxygenates is quantitatively obtained by a descriptor of the barrier difference between C₂ oxygenates (CH₂CHO) and primary by-products (CH₄ or C₂H₄) (Zhang et al., 2019; Zhang et al., 2013; Zhang et al., 2013), in which the larger the barrier difference is, the higher the selectivity of C₂ oxygenates is. As shown in Fig. 9, the energy barrier differences on the five surfaces with the Cu⁰, Cu⁺ and Cu^{δ+}(0 < δ < 1) sites correspond to the values of -40.1, 27.1, 13.3, 26.3 and 33.9 kJ.mol⁻¹, respectively, indicating that the selectivity of C₂ oxygenates follows the order of Cu/Cu₂O(1 1 1)-O_{v50} > Cu₂O(1 1 1) ≈ Cu₂O(1 1 1)-O_{v50} > Cu₂O(1 1 1)-O_{v25} > Cu(1 1 1). Moreover, the formation activity of C₂ oxygenates follows the order Cu₂O(1 1 1)-O_{v50} > Cu/Cu₂O(1 1 1)-O_{v50} > Cu(1 1 1) > Cu₂O(1 1 1) > Cu₂O(1 1 1)-O_{v25} with the corresponding overall energy barriers of 16.8, 20.0, 49.6, 70.0 and 82.9 kJ.mol⁻¹ respectively. Further, as presented in Fig. 8, the d-band center of Cu(1 1 1) surface as the Cu⁰ sites goes away from the Fermi level in comparison to the Cu⁺ and Cu^{δ+}(0 < δ < 1) sites, whereas that of Cu₂O(1 1 1)-O_{v50} and Cu/Cu₂O(1 1 1)-O_{v50} surfaces with the moderate valence state Cu^{δ+}(δ = 0.43 and 0.51) sites is more close

to the Fermi level, namely, the Cu^{δ+}(0 ≤ δ ≤ 1) sites where the d-band center is closer to the Fermi level exhibit high activity for C₂ oxygenates formation, which is similar to our results for the formation of the preferred CH_x monomer. Thus, under the reducing atmosphere of syngas conversion, once the preferred CH_x monomer is formed, for the metastable state Cu^{δ+}(0 < δ < 1) structures, the moderate valence state Cu^{δ+}(δ = 0.43 and 0.51) sites can highly-active and highly-selective catalyze the syngas conversion to produce C₂ oxygenates instead of that to produce methane and C₂ hydrocarbons.

3.5. Comparisons about Cu^{δ+}(0 ≤ δ ≤ 1) sites between the experimental and calculated results

In the experiments, considerable efforts have probed into the formation of C₂ oxygenates from syngas over Cu-based catalysts, which have indirectly confirmed our theoretical results that a moderate valence state Cu^{δ+} sites was beneficial to higher alcohols formation and the Cu^{δ+}(0 ≤ δ ≤ 1) site is determined by the ratio of Cu⁰/(Cu⁰ + Cu⁺) or Cu⁺/(Cu⁰ + Cu⁺) (Li et al., 2019; Sun et al., 2019; Yoshihara et al., 1995; Shi et al., 2017; Zuo et al., 2014; Deng et al., 2019; Yu et al., 2013; Li et al., 2017). For example, Yoshihara et al. (1995) simulated methanol synthesis over the clean polycrystalline Cu foil by kinetics method, and proved that metallic Cu was the active site for methanol synthesis on Cu/ZnO catalyst. Similarly, Shi et al. (2017) also found that the nitrogen-doped carbon-nanotube-supported Cu-Fe catalyst with a high ratio of Cu⁰/(Cu⁰ + Cu⁺) promoted CH₃OH formation. Namely, when the ratio of Cu⁰/(Cu⁰ + Cu⁺) in Cu-based catalyst is close to 1 (Cu^{δ+}(δ → 0)), methanol is the main product during syngas conversion. On the other hand, Zuo et al. (2013, 2014) prepared CuZnAl catalyst through complete liquid-phase technology and obtained Cu⁰ and Cu⁺ species on the catalyst surface by XPS characterization; for ethanol formation from syngas, it was found that the balanced Cu⁰-Cu⁺ sites on the ZnO surface are necessary for ethanol formation, while too high or too low Cu⁺ is not conducive to the formation of ethanol; moreover, the identical conclusions were also obtained by Deng et al. (2019) and Yu et al. (2013) that only when the ratio of Cu⁺/Cu⁰ was moderate, the selectivity of high alcohols increased significantly. Further, the Cu-Al oxide catalysts were synthesized by Li et al. using the impregnation method (Li et al., 2017); the results revealed that the ratio of Cu⁺/(Cu⁺+Cu⁰) has great effects on product selectivity in CO hydrogenation: methanol was obviously increased when Cu⁺/(Cu⁺+Cu⁰) is low (<0.4) or high (close to 1), ethanol was increased significantly when the ratio of Cu⁺/(Cu⁺+Cu⁰) is moderate (0.54), which is consistent with the observation from the results of direct synthesis of ethanol from CO hydrogenation over the Cu/SiO₂ catalysts prepared by ammonia vapor method (Li et al., 2019). Recently; Sun et al. (2019) designed a "spherical-plate-like" (CuMn-Co) nanosized particles structure novel CuCoMn ternary catalyst, experimental characterization found that the Mn species in the optimized CuCoMn catalyst can modified the chemical states of Cu species resulting in an appropriate ratio of surface Cu⁺/(Cu⁰ + Cu⁺) and further improve the selectivity of ethanol. Yue et al. (2014) reported that synthesizing higher alcohols from syngas required the synergistic effects of Cu⁺-Cu⁰ sites, in which Cu⁺ species acted as the stabilizer of the methoxy and acyl species, Cu⁰ species activated H₂; the appropriate amounts of Cu⁺ and Cu⁰ existed, the higher alcohols formation would be promoted.

Based on above experimental studies, it is found that the Cu^{δ+}(0 < δ < 1) sites with the moderate valence state Cu^{δ+} can promote the C-O cleavage of CH_xO, and significantly increase the amounts of CH_x species and further promote the selectivity of C₂ oxygenates. However, when the Cu^{δ+}(δ → 1) and Cu^{δ+}(δ → 0) sites with higher and lower valence state are acted as the active site in

the process of syngas conversion, the concentration of CH_xO species increased on the catalyst surface by limiting the C-O cleavage in CH_xO , then, the CH_xO species basically underwent hydrogenation to produce methanol.

In summary, taking two key steps of syngas-to- C_2 oxygenates into consideration, CO activation to produce the key CH_x intermediate and the formation of C_2 oxygenates, our results for the first time found that over the Cu-based catalysts, the Cu^+ and Cu^0 sites acted as the higher and lower valence state active sites, exhibit high selectivity of methanol instead of CH_x intermediate and C_2 oxygenates; whereas the moderate valence state $\text{Cu}^{\delta+}$ ($\delta = 0.43$ and 0.51) sites are acted as the active site, both can highly-active and highly-selective catalyze syngas conversion to produce CH_x intermediate and C_2 oxygenates instead of that to produce methanol and hydrocarbons. Therefore, in the experiment preparation of the catalyst, keeping a moderate Cu^0/Cu^+ ratio can gain high proportions of the moderate valence state $\text{Cu}^{\delta+}$ ($0 < \delta < 1$) sites to realize the balancing effect of active $\text{Cu}^{\delta+}$ ($0 < \delta < 1$) sites, contributing to excellent activity and selectivity toward the conversion of syngas-to- C_2 oxygenates; moreover, the redox properties of Cu_2O should be enhanced by doping other metal promoter, contributing to more surface oxygen-vacancies leading to surface Cu reconstruction, which is in favor of the formation of the moderate valence state $\text{Cu}^{\delta+}$ ($0 < \delta < 1$) sites. The balancing effect of active species reported here have potential to contribute to understanding the catalytic essence of Cu catalyst in the heterogeneous catalysis.

4. Conclusions

In this study, the precise role of $\text{Cu}^{\delta+}$ ($0 \leq \delta \leq 1$) sites in the conversion of syngas-to- C_2 oxygenates over the Cu catalysts is quantitatively identified using DFT calculations and microkinetic modeling. Here, the Cu^+ and Cu^0 sites were modeled using the $\text{Cu}_2\text{O}(1\ 1\ 1)$ and $\text{Cu}(1\ 1\ 1)$ surfaces, respectively; the metastable $\text{Cu}^{\delta+}$ ($0 < \delta < 1$) sites from the high to low valence state were modeled using the $\text{Cu}_2\text{O}(1\ 1\ 1)\text{-O}_{v25}$, $\text{Cu}_2\text{O}(1\ 1\ 1)\text{-O}_{v50}$ and $\text{Cu}/\text{Cu}_2\text{O}(1\ 1\ 1)\text{-O}_{v50}$ surfaces; these five surface models reflect the reduction process from the Cu^+ to Cu^0 species under the reducing atmosphere of syngas conversion. The results showed that CH_2 monomer is the preferred CH_x species on the Cu catalysts with the Cu^0 ($0 \leq \delta \leq 1$) sites, when the Cu^+ and Cu^0 sites are acted as the active site, methanol is preferably formed; whereas the moderate valence state $\text{Cu}^{\delta+}$ ($\delta = 0.43$ and 0.51) sites is more conducive to the formation of the preferred CH_2 monomer. Moreover, starting from the preferred CH_2 monomer, the moderate valence state $\text{Cu}^{\delta+}$ ($\delta = 0.43$ and 0.51) sites exhibit highly-active and highly-selective toward the conversion of syngas-to- C_2 oxygenates. Thus, the moderate valence state $\text{Cu}^{\delta+}$ ($\delta = 0.43$ and 0.51) sites dominantly contribute to the formation of C_2 oxygenates instead of $\text{CH}_3\text{-OH}$ or hydrocarbons. Further, the analysis of electronic properties well reveals this phenomenon. Therefore, under the reducing atmosphere for the conversion of syngas-to- C_2 oxygenates, the experimental preparation of Cu catalyst should focus on the high proportions of metastable $\text{Cu}^{\delta+}$ ($0 < \delta < 1$) structures with the moderate valence state $\text{Cu}^{\delta+}$ ($\delta = 0.43$ and 0.51) sites, which can be realized by adjusting the redox properties of Cu^+ species using metal promoters, contributing to more surface oxygen-vacancies leading to surface Cu reconstruction; the results of this study not only help peer scientists understand the reaction theories associated with the experimental results, but also help them advance the design of cost-effective and structure-tunable Cu-based catalysts (materials) with highly catalytic performances needed for the conversion of syngas-to- C_2 oxygenates in industry, which can have broad impact on catalyst development.

CRediT authorship contribution statement

Cong Wei: Writing - original draft, Writing - review & editing. **Riguang Zhang:** Conceptualization, Writing - original draft, Writing - review & editing, Resources, Funding acquisition, Validation. **Lixia Ling:** Formal analysis. **Debao Li:** Formal analysis. **Bo Hou:** Formal analysis. **Baojun Wang:** Data curation, Project administration, Resources, Software, Supervision.

Declaration of Competing Interest

The authors declare that they have no known competing financial interests or personal relationships that could have appeared to influence the work reported in this paper.

Acknowledgment

This work is financially supported by the National Natural Science Foundation of China (Nos. 21736007, 21776193 and 21476155), the China Scholarship Council (201606935026) and the Top Young Innovative Talents of Shanxi.

Appendix A. Supplementary material

The detailed descriptions about the computational details of the relevant energy and d -band, the scaling relationship for valence state predication, the adsorption behaviors of key intermediates, the reactions of CO activation to form CH_x intermediates, the reactions related to CH_2 species and microkinetic modeling are all presented.

Supplementary data to this article can be found online at <https://doi.org/10.1016/j.ces.2020.115785>.

References

- Behrens, M., Behrens, M., Studt, F., Kasatkin, I., Kuhl, S., Havecker, M., Abild-Pedersen, F., Zander, S., Girgsdies, F., Kurr, P., Knief, B.L., Tovar, M., Fischer, R.W., Nørskov, J.K., Schlögl, R., 2012. *Science* 336, 893–897.
- Bendavid, L.L., Carter, E.A., 2013. *J. Phys. Chem. B* 117, 15750–15760.
- Bendavid, L.L., Carter, E.A., 2013. *J. Phys. Chem. C* 117, 26048–26059.
- Cant, N.W., Tonner, S.P., Trimm, D.L., Wainwright, M.S., 1985. *J. Catal.* 91, 197–207.
- Carter, E.A., 2008. *Science* 321, 800–803.
- Chang, X.X., Wang, T., Zhao, Z.J., Yang, P.P., Greeley, J., Mu, R.T., Zhang, G., Gong, Z.M., Luo, Z.B., Chen, J., Cui, Y., Ozin, A.G., Gong, J.L., 2018. *Angew. Chem. Int. Ed.* 57, 15415–15419.
- Choi, Y., Liu, P., 2009. *J. Am. Chem. Soc.* 131, 13054–13061.
- Chuang, S.C., Goodwin Jr., J.G., Wender, I., 1985. *J. Catal.* 95, 435–446.
- Chung, M.J., Moon, D.J., Park, K.Y., Ihm, S.K., 1992. *J. Catal.* 136, 609–612.
- Delley, B., 1990. *J. Chem. Phys.* 92, 508–517.
- Deng, H.Y., Gao, Z.H., Li, Z.D., Li, H.J., Bai, N., Huang, W., 2019. *Energy Sources, Part A* 57, 1924–1934.
- Egbebi, A., Schwartz, V., Overbury, S.H., Spivey, J.J., 2010. *Catal. Today* 149, 91–97.
- Eren, B., Heine, C., Bluhm, H., Somorjai, G.A., Salmeron, M., 2015. *J. Am. Chem. Soc.* 137, 11186–11190.
- Glezakou, V.A., Jaffe, J.E., Rousseau, R., Mei, D.H., Kathmann, S.M., Albrecht, K.O., Gray, M.J., Gerber, M.A., 2012. *Top Catal.* 55, 595–600.
- Gokhale, A.A., Dumesic, J.A., Mavrikakis, M., 2008. *J. Am. Chem. Soc.* 130, 1402–1414.
- Gong, J.L., Yue, H.R., Zhao, Y.J., Zhao, S., Zhao, L., Lv, J., Wang, S.P., Ma, X.B., 2012. *J. Am. Chem. Soc.* 134, 13922–13925.
- Govind, N., Petersen, M., Fitzgerald, G., King-Smith, D., Andzelm, J., 2009. *Comput. Mater. Sci.* 28, 250–258.
- Greiner, M.T., Jones, T.E., Klyushin, A., Gericke, A.K., Schlögl, R., 2017. *J. Am. Chem. Soc.* 139, 11825–11832.
- Gupta, M., Smith, M.L., Spivey, J.J., 2011. *ACS Catal.* 1, 641–656.
- Haider, M.A., Gogate, M.R., Davis, R.J., 2009. *J. Catal.* 261, 9–16.
- Halgren, T.A., Lipscomb, W.N., 1977. *Chem. Phys. Lett.* 49, 225–232.
- Hammer, B., Nørskov, J.K., 1995. *Surf. Sci.* 343, 211–220.
- He, Z., Lin, H., He, P., Yuan, Y., 2011. *J. Catal.* 277, 54–63.
- Hindermann, J.P., Hutchings, G.J., Kiennemann, A., 1993. *Catal. Rev.: Sci. Eng.* 35, 1–127.
- Hu, P., King, D.A., Lee, M.H., Payne, M.C., 1995. *Chem. Phys. Lett.* 246, 73–78.
- Huang, W.X., 2016. *Acc. Chem. Res.* 49, 520–527.
- Islam, M.M., Diawara, B., Maurice, V., Marcus, P., 2009. *J. Mol. Struct.: Theochem.* 903, 41–48.

- Kapur, N., Yun, J.H., Shan, B., Nicholas, J.B., Cho, K., 2010. *J. Phys. Chem. C* 114, 10171–10182.
- Kuld, S., Thorhauge, M., Falsig, H., Elkjær, C.F., Helveg, S., Chorkendorff, I., Sehested, J., 2016. *Science* 352, 969–974.
- Li, X.L., Zhang, Q.D., Xie, H.J., Gao, X.F., Wu, Y.Q., Yang, G.H., Wang, P., Tian, S.P., Tan, Y.S., 2017. *ChemistrySelect* 2, 10365–10370.
- Li, X.L., Yang, G.H., Zhang, M., Gao, X.F., Xie, H.J., Bai, Y.X., Wu, Y.Q., Pan, J.X., Tan, Y.S., 2019. *ChemCatChem* 11, 1123–1130.
- Lin, J., May, J.A., Didziulis, S.V., Solomon, E.I., 1992. *J. Am. Chem. Soc.* 114, 4718–4727.
- Liu, H.X., Zhang, R.G., Ling, L.X., Wang, Q., Wang, B.J., Li, D.B., 2017. *Catal. Sci. Technol.* 7, 3758–3776.
- Maimaiti, Y., Nolan, M., Elliott, S.D., 2014. *Phys. Chem. Chem. Phys.* 16, 3036–3046.
- Mei, D.H., Rousseau, R., Kathmann, S.M., Glezakou, V.A., Engelhard, M.H., Jiang, W.L., Wang, C.M., Gerber, M.A., White, J.F., Stevens, D.J., 2010. *J. Catal.* 271, 325–342.
- Mo, X.H., Gao, J., Umnajkaseam, N., Goodwin Jr., J.G., 2009. *J. Catal.* 267, 167–176.
- Morrill, M.R., Thao, N.T., Shou, H., Davis, R.J., Barton, D.G., Ferrari, D., Agrawal, P.K., Jones, C.W., 2013. *ACS Catal.* 3, 1665–1675.
- Nie, X., Griffin, G.L., Janik, M.J., Asthagiri, A., 2014. *Catal. Commun.* 52, 88–91.
- Nilius, N., Fedderwitz, H., Grob, B., Noguera, C., Goniakowski, J., 2016. *Phys. Chem. Chem. Phys.* 18, 6729–6733.
- Önsten, A., Göthelid, M., Karlsson, U.O., 2009. *Surf. Sci.* 603, 257–264.
- Pan, X.L., Fan, Z.L., Chen, W., Ding, Y.J., Luo, H.Y., Bao, X.H., 2007. *Nat. Mater.* 6, 507–511.
- Prieto, G., Beijer, S., Smith, M.L., He, M., Au, Y., Wang, Z., Bruce, D.A., de Jong, K.P., Spivey, J.J., de Jongh, P.E., 2014. *Angew. Chem. Int. Ed.* 53, 6397–6401.
- Sá, S., Silva, H., Brandão, L., Sousa, J.M., Mendes, A., 2010. *Appl. Catal. B: Environ.* 99, 43–57.
- San, X.G., Zhang, Y., Shen, W.J., Tsubaki, N., 2009. *Energy Fuels* 23, 2843–2844.
- Schulz, K.H., Cox, D.F., 1991. *Phys. Rev. B* 43, 1610–1621.
- Schumann, J., Medford, A.J., Yoo, J.S., Zhao, Z.J., Bothra, P., Cao, A., Studt, F., Pedersen, F.A., Nørskov, J.K., 2018. *ACS Catal.* 8, 3447–3453.
- Shetty, S., Santen, R.A., Stevens, P.A., Raman, S., 2010. *J. Mol. Catal. A: Chem.* 330, 73–87.
- Shi, X.P., Yu, H.B., Gao, S., Li, X.Y., Fang, H.H., Li, R.J., Li, Y.Y., Zhang, L.J., Liang, X.L., Yuan, Y.Z., 2017. *Fuel* 210, 241–248.
- Su, J.J., Zhang, Z.P., Fu, D.L., Liu, D., Xu, X.C., Shi, B.F., Wang, X., Si, R., Jiang, Z., Xu, J., Han, Y.F., 2016. *J. Catal.* 336, 94–106.
- Subramani, V., Gangwal, S.K., 2008. *Energy Fuels* 22, 814–839.
- Subramanian, N.D., Gao, J., Mo, X.H., Goodwin Jr., J.G., Torres, W., Spivey, J.J., 2010. *J. Catal.* 272, 204–209.
- Sun, J., Cai, Q.X., Wan, Y., Wan, S.L., Wang, L., Lin, J.D., Mei, D.H., Wang, Y., 2016. *ACS Catal.* 6, 5771–5785.
- Sun, B.Z., Chen, W.K., Wang, X., Lu, C.H., 2007. *Appl. Surf. Sci.* 253, 7501–7505.
- Sun, B.Z., Chen, W.K., Zheng, J.D., Lu, C.H., 2008. *Appl. Surf. Sci.* 255, 3141–3148.
- Sun, K., Tan, M.H., Bai, Y.X., Gao, X.F., Wang, P., Gong, N.N., Zhang, T., Yang, G.H., Tan, Y.S., 2019. *J. Catal.* 78, 1–16.
- Sun, X.C., Zhang, R.G., Wang, B.J., 2013. *Appl. Surf. Sci.* 265, 720–730.
- Sun, X.C., 2013. *Study on the reaction mechanism of ethanol synthesis from on Cu catalyst*, Ms. D. Thesis, Taiyuan University of Technology, (2013) June..
- Sung, S.S., Hoffmann, R., 1985. *J. Am. Chem. Soc.* 107, 578–584.
- Tian, D.X., Zhang, H.L., Zhao, J.J., 2007. *Solid State Commun.* 144, 174–179.
- Tissot, H., Wang, C.L., Stenlid, J.H., Panahi, M., Kaya, S., Soldemo, M., Yazdi, M.G., Brinck, T., Weissenrieder, J., 2019. *J. Phys. Chem. C* 123, 22172–22180.
- Wang, P., Chen, S.Y., Bai, Y.X., Gao, X.F., Li, X.L., Sun, K., Xie, H.J., Yang, G.H., Han, Y.Z., Tan, Y.S., 2017. *Fuel* 195, 69–81.
- Wang, W.W., Du, P.P., Zou, S.H., He, H.Y., Wang, R.X., Jin, Z., Shi, S., Huang, Y.Y., Si, R., Song, Q.S., Jia, C.J., Yan, C.H., 2015. *ACS Catal.* 5, 2088–2099.
- Wang, Y., Shen, Y.L., Zhao, Y.J., Lv, J., Wang, S.P., Ma, X.B., 2015. *ACS Catal.* 5, 6200–6208.
- Xiang, Y.Z., Barbosa, R., Li, X.N., Kruse, N., 2015. *ACS Catal.* 5, 2929–2934.
- Yang, N.Y., Medford, A.J., Liu, X.Y., Studt, F., Bligaard, T., Bent, S.F., Nørskov, J.K., 2016. *J. Am. Chem. Soc.* 138, 3705–3714.
- Yang, P.P., Zhao, Z.J., Chang, X.X., Mu, R.T., Zha, S.J., Zhang, G., Gong, J.L., 2018. *Angew. Chem. Int. Ed.* 57, 7724–7728.
- Yin, H.M., Ding, Y.J., Luo, H.Y., Yan, L., Wang, T., Lin, L.W., 2003. *Energy Fuels* 17, 1401–1406.
- Yin, A.Y., Guo, X.Y., Dai, W.L., Li, H.X., Fan, K.N., 2008. *Appl. Catal. A: Gen.* 349, 91–99.
- Yin, A.Y., Guo, X.Y., Dai, W.L., Fan, K.N., 2009. *J. Phys. Chem. C* 113, 11003–11013.
- Yin, A.Y., Guo, X.Y., Fan, K.N., Dai, W.L., 2010. *ChemCatChem* 2, 206–213.
- Yin, S.X., Ma, X.Y., Ellis, D.E., 2007. *Surf. Sci.* 601, 2426–2437.
- Yoshihara, J., Parker, S.C., Schafer, A., Campbell, C.T., 1995. *Catal. Lett.* 31, 313–324.
- Yu, S.R., Chen, Y.E., Gao, S.S., Wang, X.D., Huang, W., 2013. *Energy Sources, Part A* 35, 955–961.
- Yue, H.R., Zhao, Y.J., Zhao, S., Wang, B., Ma, X.B., Gong, J.L., 2013. *Nat. Commun.* 4, 2339–2345.
- Yue, H.R., Ma, X.B., Gong, J.L., 2014. *Acc. Chem. Res.* 47, 1483–1492.
- Zhang, R.G., Wang, B.J., Ling, L.X., Liu, H.Y., Huang, W., 2010. *Appl. Surf. Sci.* 257, 1175–1180.
- Zhang, R.G., Liu, H.Y., Zheng, H.Y., Ling, L.X., Li, Z., Wang, B.J., 2011. *Appl. Surf. Sci.* 257, 4787–4794.
- Zhang, R.G., Wang, B.J., Liu, H.Y., Ling, L.X., 2011. *J. Phys. Chem. C* 115, 19811–19818.
- Zhang, R.G., Liu, H.Y., Wang, B.J., Ling, L.X., 2012. *Appl. Catal. B: Environ.* 126, 108–120.
- Zhang, R.G., Sun, X.C., Wang, B.J., 2013. *J. Phys. Chem. C* 117, 6594–6606.
- Zhang, R.G., Wang, G.R., Wang, B.J., 2013. *J. Catal.* 305, 238–255.
- Zhang, R.G., Li, J.R., Wang, B.J., Ling, L.X., 2013. *Appl. Surf. Sci.* 279, 260–271.
- Zhang, R.G., Wen, G.X., Adidharma, H., Russell, A.G., Wang, B.J., Radosz, M., Fan, M.H., 2017. *ACS Catal.* 7, 8285–8295.
- Zhang, R.G., Wei, C., Li, D.B., Jiang, Z., Wang, B.J., Ling, L.X., Fan, M.H., 2019. *J. Catal.* 377, 1–12.
- Zhao, Y.H., Sun, K.J., Ma, X.F., Liu, J.X., Sun, D.P., Su, H.Y., Li, W.X., 2011. *Angew. Chem. Int. Ed.* 123, 5447–5450.
- Zhao, S., Yue, H.R., Zhao, Y.J., Wang, B., Geng, Y.C., Lv, J., Wang, S.P., Gong, J.L., Ma, X. B., 2013. *J. Catal.* 297, 142–150.
- Zheng, H.Y., Zhang, R.G., Li, Z., Wang, B.J., 2015. *J. Mol. Catal. A: Chem.* 404–405, 115–130.
- Zheng, J.W., Zhou, J.F., Lin, H.Q., Duan, X.P., Williams, C.T., Yuan, Y.Z., 2015. *J. Phys. Chem. C* 119, 13758–13766.
- Zhou, C.G., Wu, J.P., Nie, A., Forrey, R.C., Tachibana, A., Cheng, H.S., 2007. *J. Phys. Chem. C* 111, 12773–12778.
- Zuo, Z.J., Wang, L., Liu, Y.J., Huang, W., 2013. *Catal. Commun.* 34, 69–72.
- Zuo, Z.J., Wang, L., Yu, L.M., Han, P.D., Huang, W., 2014. *J. Phys. Chem. C* 118, 12890–12898.